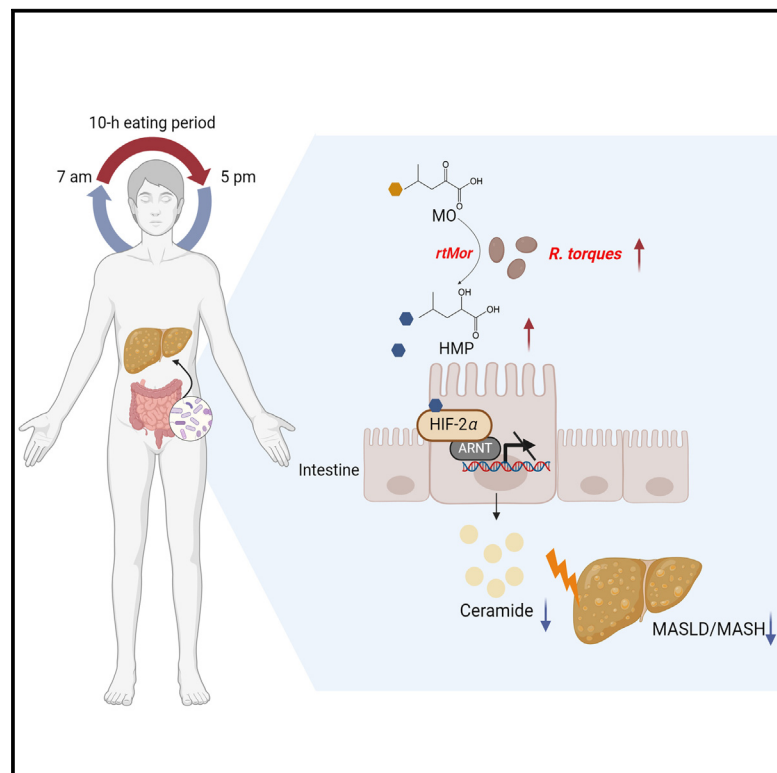


Cell Metabolism

A microbial metabolite inhibits the HIF-2 α -ceramide pathway to mediate the beneficial effects of time-restricted feeding on MASH

Graphical abstract



Authors

Yi Zhang, Xuemei Wang, Jun Lin, ..., Wei Fu, Changtao Jiang, Yanli Pang

Correspondence

wanguangcy@ccmu.edu.cn (G.W.), zhangzhipeng06@126.com (Z.Z.), fuwei@bjmu.edu.cn (W.F.), jiangchangtao@bjmu.edu.cn (C.J.), yanlipang@bjmu.edu.cn (Y.P.)

In brief

Zhang et al. discover that TRF improves metabolic dysfunction-associated steatotic liver disease/metabolic dysfunction-associated steatohepatitis (MASLD/MASH) through modulating gut-liver crosstalk. Mechanistically, *R. torques* is significantly increased after TRF, modulates the synthesis of HMP via *rtMor*, inhibits the HIF-2 α -ceramide pathway, and improves MASLD/MASH. These findings offer potential probiotic intervention strategies for MASLD/MASH.

Highlights

- TRF-associated bacteria *R. torques* ameliorates MASLD/MASH via its metabolite HMP
- *rtMor* is an enzyme identified in *R. torques* that generates HMP generation
- HMP can serve as a TRF mimetic, addressing poor adherence to fasting regimens



Article

A microbial metabolite inhibits the HIF-2 α -ceramide pathway to mediate the beneficial effects of time-restricted feeding on MASH

Yi Zhang,^{1,2,16} Xuemei Wang,^{3,4,16} Jun Lin,^{3,4,5,16} Jia Liu,^{5,16} Kai Wang,^{3,4} Qixing Nie,^{3,4} Chuan Ye,^{3,4} Lulu Sun,^{6,7} Yanpeng Ma,^{1,2} Ruize Qu,^{1,2} Yuejian Mao,⁹ Xuguang Zhang,^{9,10} Hua Lu,¹¹ Pengyan Xia,¹² Dongyu Zhao,^{3,13} Guang Wang,^{5,*} Zhipeng Zhang,^{1,2,*} Wei Fu,^{1,2,*} Changtao Jiang,^{3,4,14,15,*} and Yanli Pang^{7,8,17,*}

¹Department of General Surgery, Cancer Center, Peking University Third Hospital, Beijing, China

²Center of Basic Medical Research, Institute of Medical Innovation and Research, Third Hospital, Peking University, Beijing, China

³Department of Physiology and Pathophysiology, School of Basic Medical Sciences, State Key Laboratory of Vascular Homeostasis and Remodeling, Peking University, Beijing, China

⁴Center for Obesity and Metabolic Disease Research, School of Basic Medical Sciences, Peking University, Beijing, China

⁵Department of Endocrinology, Capital Medical University Chaoyang Hospital, Beijing, China

⁶Department of Endocrinology and Metabolism, Peking University Third Hospital, Beijing, China

⁷State Key Laboratory of Female Fertility Preservation, Center for Reproductive Medicine, Department of Obstetrics and Gynecology, Peking University Third Hospital, Beijing, China

⁸National Clinical Research Center for Obstetrics and Gynecology, Peking University Third Hospital, Beijing, China

⁹Mengniu Institute of Nutrition Science, Shanghai, China

¹⁰Shanghai Institute of Nutrition and Health, The Chinese Academy of Sciences, Shanghai, China

¹¹National Laboratory for Molecular Sciences, Center for Soft Matter Science and Engineering, Key Laboratory of Polymer Chemistry and Physics of Ministry of Education, College of Chemistry and Molecular Engineering, Peking University, Beijing, China

¹²Department of Immunology, School of Basic Medical Sciences, Peking University, Beijing, China

¹³Department of Biomedical Informatics, School of Basic Medical Sciences, Peking University Health Science Center, Beijing, China

¹⁴Department of Immunology, School of Basic Medical Sciences, State Key Laboratory of Female Fertility Promotion, Peking University, Beijing, China

¹⁵NHC Key Laboratory of Medical Immunology, Peking University, Beijing, China

¹⁶These authors contributed equally

¹⁷Lead contact

*Correspondence: wangguangcy@ccmu.edu.cn (G.W.), zhangzhipeng06@126.com (Z.Z.), fuwei@bjmu.edu.cn (W.F.), jiangchangtao@bjmu.edu.cn (C.J.), yanlipang@bjmu.edu.cn (Y.P.)
<https://doi.org/10.1016/j.cmet.2024.07.004>

SUMMARY

Time-restricted feeding (TRF) is a potent dietary intervention for improving metabolic diseases, including metabolic dysfunction-associated steatotic liver disease/metabolic dysfunction-associated steatohepatitis (MASLD/MASH). However, the mechanism of this efficacy has remained elusive. Here, we show that TRF improves MASLD, which is associated with a significant enrichment of *Ruminococcus torques* (*R. torques*). Mechanistically, *R. torques* suppresses the intestinal HIF-2 α -ceramide pathway via the production of 2-hydroxy-4-methylpentanoic acid (HMP). We identify *rtMor* as a 4-methyl-2-oxopentanoate reductase that synthesizes HMP in *R. torques*. Finally, we show that either the colonization of *R. torques* or oral HMP supplementation can ameliorate inflammation and fibrosis in a MASH mouse model. These findings identify *R. torques* and HMP as potential TRF mimetics for the treatment of metabolic disorders.

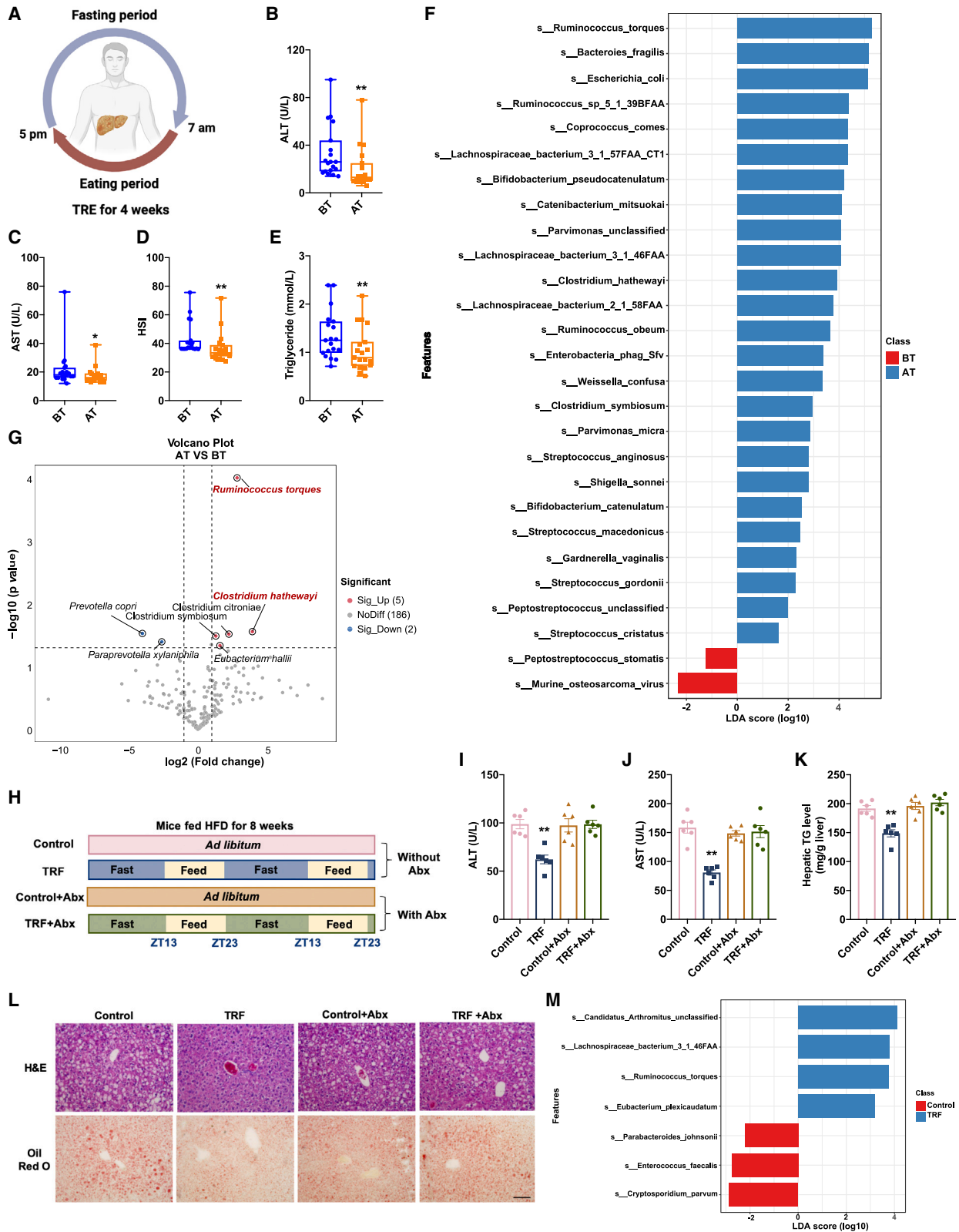
INTRODUCTION

Metabolic dysfunction-associated steatotic liver disease (MASLD), which affects a quarter of the population, poses a major health and economic burden to all societies.¹ MASLD encompasses a diverse range of hepatic manifestations, which vary from liver steatosis to the more aggressive metabolic dysfunction-associated steatohepatitis (MASH), the latter of which is hallmarked by necroinflammation and fibrosis that can progress to cirrhosis

and hepatocellular carcinoma (HCC).² Slowing the progression of MASLD, and in particular reversing established MASH, is the focus of clinical treatment. In view of its complex pathology and the current lack of approved medical interventions, aggressive dietary and lifestyle approaches remain the leading options for its management but are limited due to poor adherence.^{3,4}

Adjusting dietary intake, as well as meal frequency and the dietary time window, have become powerful tools to improve and delay disease onset and aging.⁵ Time-restricted feeding (TRF),





(legend on next page)

which entails restricting daily food consumption to a 4- to 12-h window without limiting caloric intake, is considered a potent dietary and lifestyle intervention to ameliorate and postpone the onset of disease. Studies have shown that TRF can reduce body weight, improve insulin resistance, and suppress liver lipid accumulation.^{6–8} However, the specific molecular mechanisms responsible for the benefits of TRF are still elusive.

The composition of the gut microbiota is a key factor in the regulation of host metabolism. The shape and function of the gut microbiota are susceptible to dietary characteristics, such as the amount and composition of lipids. Food overconsumption, food shortage, and even changes in the eating cycle may affect the gut microbiota.^{9–11} TRF can partially restore the periodic fluctuation of the gut microbiota caused by high-fat diet (HFD) feeding in mice, increasing the diversity of the gut microbiota and affecting host metabolism,¹¹ suggesting that the gut microbiota may play an important role in the benefits of TRF. Microbial metabolites are recognized as the key mediators of communication between the microbiota and the host, maintaining the physiological function of the host.¹² Whether the gut microbiota and microbial metabolites contribute to the effect of TRF on MASLD/MASH remains to be explored.

In this study, we utilized a 10-h TRF regimen as an intervention in patients with MASLD and in mouse models to explore the underlying mechanisms by which TRF can ameliorate this condition. We found that *Ruminococcus torques* (*R. torques*) in the gut microbiota was increased after 10-h TRF and that colonization with this species was sufficient to simulate the beneficial effects of TRF on MASLD/MASH. Mechanistically, we found that *R. torques* improved MASLD/MASH by inhibiting the intestinal HIF-2 α -ceramide axis through its microbial metabolite, 2-hydroxy-4-methylpentanoic acid (HMP). Collectively, these results establish the role of *R. torques* and one of its associated metabolites, HMP, in the beneficial effects of TRF on MASLD/MASH, suggesting that *R. torques* or HMP may be developed as a probiotic or as a pharmacological treatment for MASLD/MASH.

RESULTS

Changes in the gut microbiota mediate the benefits of TRF for MASLD

To explore the potential benefits of time-restricted eating (TRE) for MASLD, we enrolled 19 participants with MASLD in a clinical intervention study involving a 4-week TRE regimen in which par-

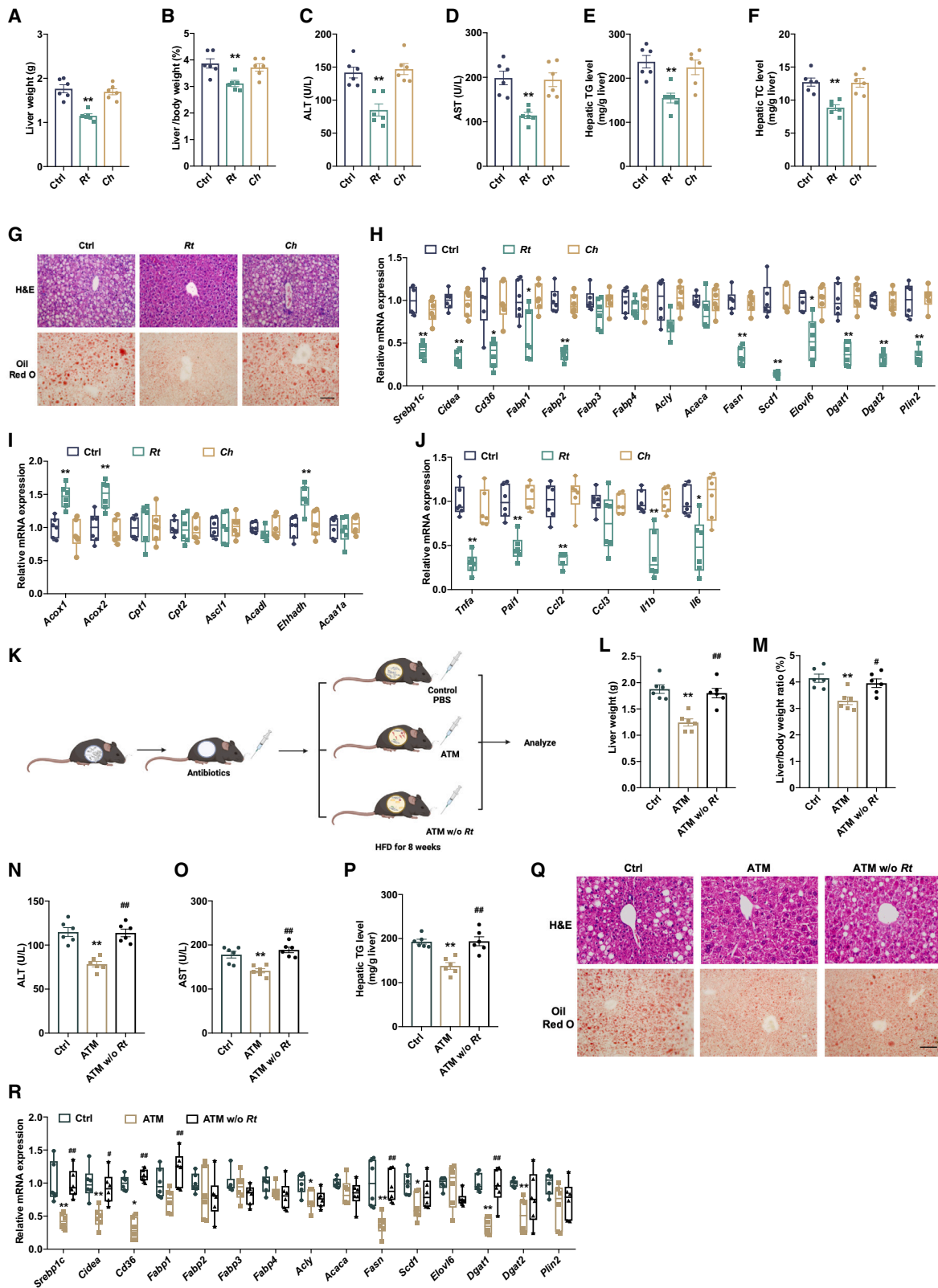
ticipants were instructed to eat *ad libitum* from 7 a.m. to 5 p.m. (10-h eating) and to fast from 5 p.m. to 7 a.m. (14-h fasting) daily (Figure 1A). During the study period, feces and plasma samples were collected before and after TRE. Considering that liver function and dyslipidemia show clear biological links to the progression of MASLD,² representative indicators of liver function and dyslipidemia were detected (Table S1). Plasma alanine aminotransferase (ALT), aspartate aminotransferase (AST), and gamma-glutamyltransferase (GGT), reflecting the degree of liver damage, were obviously decreased after 4 weeks of a TRE (AT) regimen, while alkaline phosphatase (ALP) showed no significant difference compared with those levels before TRE (BT) (Figures 1B, 1C, S1A, and S1B). A hepatic steatosis index (HSI) ≥ 36 is an indicator of MASLD. After TRE, participants with MASLD had significantly lower HSI indices (Figure 1D). Accordingly, serum triglyceride (TG) levels were also markedly reduced by TRE, accompanied by a decreased body weight index (BMI) (Figures 1E and S1C).

To determine the individual-specific dynamic changes in the gut microbiota induced by TRE, we performed whole-genome shotgun sequencing of stool samples collected from the participants before and after TRE study. The α -diversity was slightly increased after the TRE intervention (Figures S1D–S1F), and the composition and abundance of the gut microbiota between the two groups showed significant differences (principal coordinates analysis [PCoA], p value = 0.009, Figure S1G). By LefSe analysis, we found that the abundance of *R. torques*, belonging to the order *Clostridiales*, was significantly increased after TRE (Figure 1F). Accordingly, the volcano plot also indicated that *R. torques* is the most significant increased strain after TRE intervention, followed by *Clostridium hathewayi* (*C. hathewayi*, Figure 1G).

To verify the effect of TRF on the development of HFD-induced MASLD and the role of the gut microbiota during a TRF intervention, 8-week-old male C57BL/6J mice fed HFD *ad libitum* or only during a 10-h TRF (from ZT13 to ZT23) regimen for 8 weeks, combined with or without an antibiotic cocktail (Abx) treatment (Figure 1H). The TRF group showed lower ALT and AST levels (Figures 1I and 1J), as well as reduced body weights, liver weights, and liver/body weight ratios (Figures S1H–S1J) compared with the control group. The TG and TC levels in plasma and liver were decreased, when compared with the control group (Figures 1K and S1K–S1M). By H&E and oil red O staining, we found that TRF improved liver steatosis in the HFD-induced MASLD mouse model (Figures 1L and S1N). Moreover, the mRNA expression of

Figure 1. Changes in the gut microbiota are associated with the benefits of TRF for MASLD

(A) Clinical experimental design. Participants are allowed to eat *ad libitum* from 7 a.m. to 5 p.m. and are restricted from 5 p.m. to 7 a.m. the next day. The TRE regime lasted for 4 weeks.
(B–E) ALT (B), AST (C), HSI (D), and serum triglyceride (E) levels of participants before and after TRE intervention.
(F) The linear discriminant analysis (LDA) effect size (LefSe) was conducted to identify the differentially abundant bacteria among the baseline and TRE groups.
(G) Volcano map of gut microbiota before and after TRE intervention.
(H) TRF experimental design of mice. Mice were allowed to eat *ad libitum* from ZT13 to ZT23 and restricted from ZT23 to ZT13. ZT0 means light on.
(I–K) ALT (I), AST (J), and hepatic TG (K) levels of mice.
(L) Representative H&E (top) and oil red O (bottom) staining of liver section from the indicated groups of mice. Scale bars, 100 μ m.
(M) The linear discriminant analysis (LDA) effect size (LefSe) was conducted to identify the differentially abundant bacteria among the control and TRF groups. $n = 19$ per group (A–F); $n = 6$ per group (I–K); $n = 5$ per group (M). Data are shown as first and third quartiles in box and whiskers (B–E) and mean \pm SEM (I–K) and the median with first. p values were determined by Wilcoxon's sign rank test (B–D), paired t test (E), and one-way analysis of variance (ANOVA) with Tukey post hoc test (I–K). In (B)–(E), $^*p < 0.05$ and $^{**}p < 0.01$ versus the BT group. In (I)–(K), $^{**}p < 0.01$ versus the control group. Abx, antibiotic cocktail; ALT, alanine aminotransferase; AT, after TRF; AST, aspartate aminotransferase; BT, before TRF; H&E, hematoxylin-eosin staining; HSI, hepatorenal steatosis index; TG, triglyceride; TRE, time-restricted eating; TRF, time-restricted feeding.



(legend on next page)

genes involved in fatty acid transport, lipogenesis, and inflammation was substantially reduced, while the mRNA expression of genes involved in fatty acid β -oxidation was increased in the TRF group (Figures S1O–S1Q). However, TRF-mediated improvements were abolished by Abx treatment (Figures 1I–1L and S1H–S1Q), suggesting the important role of the gut microbiota during TRF intervention.

Next, we performed whole-genome shotgun sequencing of the control and TRF group. The α -diversity and β -diversity showed no statistical difference between the two groups (Figures S1R–S1U). By LEfSe analysis, we found that abundance of *R. torques* was noticeably increased in the TRF group, in accordance with the changes in the human samples (Figure 1M).

***R. torques* is the key bacterial species that contributes to the benefits of TRF for MASLD**

To verify which bacterial strain primarily mediates TRF-induced amelioration of MASLD, we investigated the role of *R. torques* and *C. hathewayi* in the progression of MASLD. Mice gavaged with *R. torques* had lower body weights, liver weights, and liver/body weight ratios compared with the control group (Figures 2A, 2B, and S2A), accompanied by improvements in plasma and hepatic TG and TC levels, and ALT and AST levels (Figures 2C–2F, S2B, and S2C). Furthermore, by H&E and oil red O staining, we found a reduction in hepatic lipid droplets in the *R. torques* group compared with control group (Figures 2G and S2D). The mRNA expression of genes involved in fatty acid transport, lipogenesis, and inflammation was substantially reduced, while the mRNA expression of genes involved in fatty acid β -oxidation was increased in the *R. torques* group (Figures 2H–2J). However, *C. hathewayi* treatment failed to improve any indicator of MASLD, including plasma and hepatic TG and TC levels and ALT and AST levels (Figures 2A–2J and S2A–S2D). These data indicate that *R. torques* supplementation can alleviate HFD-induced MASLD. In addition, in a clinical trial, the abundance of *R. torques* showed a negative correlation with HSI (Figure S2E).

Given the critical effect of *R. torques* in mediating the clinical benefit of TRF, we mixed the top ten bacterial species of the AT group as a model microbiome, which we referred to as “after TRF microbes” (ATM) (Figure S2F). Then, we colonized mice with ATM or ATM without *R. torques* (ATM w/o *Rt*) by gavage to confirm the contribution of *R. torques* to the progression of MASLD (Figure 2K). Body weights, liver weights, and liver/body

weight ratios were decreased, with lower plasma ALT and AST levels in the ATM group compared with ATM w/o *Rt* group (Figures 2L–2O and S2G). Likewise, by H&E and oil red O staining, we found that mice in the ATM group showed improved hepatic steatosis and reduced plasma and hepatic TG and TC levels compared with ATM w/o *Rt* group (Figures 2P, 2Q, and S2H–S2K). The mRNA expression of genes involved in fatty acid transport, lipogenesis, and inflammation was substantially reduced, while the mRNA expression of genes involved in fatty acid β -oxidation was increased in mice receiving the ATM (Figures 2R, S2L, and S2M). The results of 16S ribosomal RNA confirmed that bacterial species successfully colonized, and the stool of ATM w/o *Rt* group contained little *R. torques* (Figure S2N). However, removing *R. torques* from ATM eliminated the protective effects of ATM gavage, indicating that *R. torques* mediates the clinical benefit of TRF.

***R. torques* improves MASLD by inhibiting intestinal HIF-2 α**

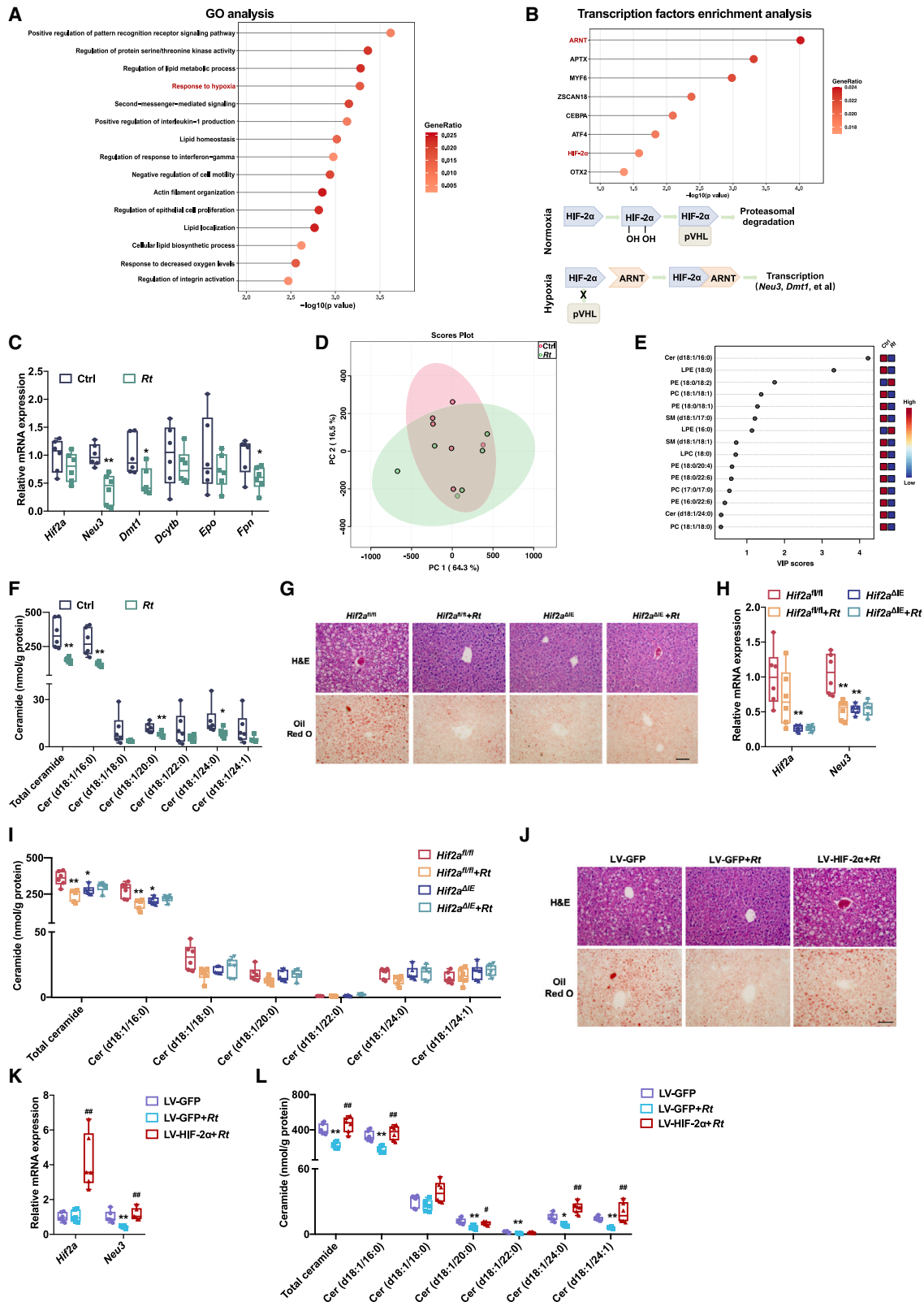
To explore the mechanism underlying the metabolic benefits induced by *R. torques* supplementation, we performed transcriptome analysis via RNA sequencing (RNA-seq) of intestinal epithelia from *R. torques*-gavaged mice and PBS-gavaged mice. By Gene Ontology (GO) analysis, we found that several pathways showed significant changes, including lipid metabolic process and response to hypoxia (Figure 3A). Transcription factors enrichment analysis indicated that hypoxia-inducible factor (HIF)- β (HIF- β , also known as ARNT)- and HIF-2 α -mediated transcriptional activation may play important roles in *R. torques*-mediated metabolic benefits of MASLD. In states of normoxia, HIF-2 α is hydroxylated by prolyl hydroxylase domain (PHD) and subsequently degraded.¹³ However, during hypoxia, the activity of PHD is inhibited, and HIF-2 α physically interacts with ARNT, regulating the transcription of downstream genes (Figure 3B). Consistent with this pathway, the mRNA expressions of the *Hif2a*-related downstream genes *Neu3*, *Dmt1*, and *Fpn* showed a significant decrease in *R. torques*-gavaged mice compared with PBS-gavaged mice (Figure 3C).

Intestinal HIF-2 α -ceramide signaling axis mediates the beneficial effects of *R. torques*

Our previous study has found that intestinal HIF-2 α upregulates the expression of *Neu3*, increases ceramide synthesis, and

Figure 2. *R. torques* is the key bacterial species that contributes to the benefits of TRF for MASLD

(A–F) Liver weights (A), liver/body weight ratio (B), ALT levels (C), AST levels (D), hepatic TG levels (E), and hepatic TC levels (F) of mice treated with an HFD combined with *R. torques* or *C. hathewayi* for 8 weeks.
(G) Representative H&E (top) and oil red O (bottom) staining of liver section from the indicated groups of mice. Scale bars, 100 μ m.
(H–J) Relative mRNA expressions of the indicated genes related to hepatic fatty acid transport and lipogenesis-related genes (H), fatty acid β -oxidation-related genes (I), and inflammatory cytokine and chemokine genes (J).
(K) The schematic diagram of the mice experiment gavaged by ATM or ATM w/o *Rt*: specific pathogen-free mice were pretreated with antibiotics for 3 days, then gavaged by PBS (Ctrl), AT microbes (ATM), or ATM without *R. torques* (ATM w/o *Rt*) for 8 weeks.
(L–P) Liver weights (L), liver/body weight ratio (M), ALT levels (N), AST levels (O), and hepatic TG levels (P) of mice.
(Q) Representative H&E (top) and oil red O (bottom) staining of liver section from the indicated groups of mice. Scale bars, 100 μ m.
(R) Relative mRNA expressions of the indicated genes related to hepatic fatty acid transport and lipogenesis-related genes.
 $n = 6$ per group. Data are shown as mean \pm SEM (A–F and L–P) and the median with first and third quartiles in box and whiskers (H–J and R). p values were determined by one-way ANOVA with Tukey post hoc test (B, C, E, F, and L–P), one-way ANOVA with Dunnett’s T3 post hoc test (D and I), and Kruskal-Wallis test with Dunn’s test (H, J, and R). In (A)–(F) and (H)–(J), * $p < 0.05$ and ** $p < 0.01$ versus the control group. In (L)–(P) and (R), * $p < 0.05$ and ** $p < 0.01$ versus the control group and # $p < 0.05$ and ## $p < 0.01$ versus the ATM group. ALT, alanine aminotransferase; AST, aspartate aminotransferase; Ctrl, control; H&E, hematoxylin-eosin staining; *Rt*, *R. torques*; TC, total cholesterol; TG, triglyceride.



(legend on next page)

aggravates MASLD development.¹⁴ Based on the RNA-seq analysis and our previous work, we then performed lipidomics analysis and found that the intestinal lipid profiles differed between the two groups (Figure 3D). Among them, ceramide levels were downregulated in the *R. torques*-treated group, especially ceramide (d18:1/16:0), the most abundant ceramide in the intestinal epithelia (Figures 3E, 3F, and S2O). Furthermore, *R. torques* treatment inhibited ceramide synthesis via the SMase pathway and salvage pathway, but it did not affect the *de novo* pathway and metabolism pathway (Figures S2P–S2S). Likewise, ATM gavage reduced the expression of *Neu3* and the concentration of ceramide in the intestine, while ATM w/o *Rt* gavage failed to change the expression of *Neu3* and the concentration of ceramide in the intestine (Figures S2T and S2U).

To explore whether the beneficial effect of *R. torques* on MASLD relied on body weight loss, we investigated the role of *R. torques* in the early stage of MASLD by exploring the effects in mice fed an HFD for 2 weeks. In the absence of any body weight change, hepatic TG levels and intestinal ceramide levels were lower in the *R. torques* treatment group compared with the control group (Figures S2V–S2X). These results verified that *R. torques* treatment reduced ceramide levels and hepatic TG levels before the onset of a change in body weight.

Next, to explore whether intestinal HIF-2 α -ceramide signaling mediates the beneficial effects of *R. torques* on MASLD, we administered *R. torques* to the intestine-specific HIF-2 α knockout (*Hif2a*^{dIE}) mice and control littermates (*Hif2a*^{fl/fl}) mice with HFD feeding and found that the *R. torques* treatment improved hepatic morphology, reduced liver weights, body weights, and the liver/body weight ratio in *Hif2a*^{fl/fl} mice, but not in *Hif2a*^{dIE} mice (Figures 3G, S3A–S3C, and S3J). *Hif2a*^{fl/fl} mice had lower plasma and hepatic TG and TC levels, ALT, and AST levels with *R. torques* treatment, as well as hepatic fatty acid transport, lipogenesis, inflammation, and fatty acid β -oxidation, but *Hif2a*^{dIE} mice had no improvement upon *R. torques* treatment (Figures S3D–S3I and S3K–S3M). Similarly, *R. torques* administration reduced the expressions of *Neu3* and intestinal ceramide levels, whereas *Hif2a*^{dIE} mice were unresponsive to *R. torques* treatment (Figures 3H and 3I). Furthermore, the ileum was incubated with an HIF-2 α -expressing lentivirus (LV-HIF-2 α) to overexpress HIF-2 α in the intestine. We found that HIF-2 α overexpression eliminated the beneficial ef-

fects of *R. torques* administration (Figures 3J–3L and S3N–S3Z). Collectively, these observations indicate that the HIF-2 α -ceramide axis is responsible for the beneficial effects of *R. torques* supplementation on MASLD.

HMP acts as an endogenous inhibitor for HIF-2 α

Evidence is accumulating that various microbial metabolites are involved in the etiology of obesity and obesity-related diseases, such as MASLD and type 2 diabetes.^{15,16} To identify the secreted molecule(s) responsible for *R. torques*-mediated inhibition of HIF-2 α function, we separated *R. torques* culture medium into two molecular mass fractions using 1 kDa ultrafiltration centrifugal tube (molecular mass cutoff membranes).¹⁷ The <1 kDa fraction of *R. torques* culture medium inhibited the HIF-2 α transcriptional activity, whereas the >1 kDa fraction failed to have any significant effects (Figure 4A). According to the Metabolomics Data Explorer (https://sonnenburglab.github.io/Metabolomics_Data_Explorer),¹⁸ 10 metabolites produced by *R. torques* with a >2-fold change in relative abundance compared with media blank controls were selected. These metabolites include HMP, 2'-deoxyguanosine 5'-monophosphate (DM), cytidine 3'-monophosphate, 3-phosphoglyceric acid (3-PA), 2'-deoxyadenosine 5'-monophosphate, fructose 1,6-biphosphate (FBP), fructose 6-phosphate (F6P), guanosine 5-monophosphate (G5M), O-phospho-serine (OPS), and thymine. By luciferase assay to measure HIF-2 α activity, we found that HMP treatment led to a dose-dependent inhibition (Figures 4B and 4C). By co-immunoprecipitation assays and mammalian two-hybrid analysis, we found that HMP disrupted the HIF-2 α -ARNT interaction (Figures 4D–4F). Furthermore, we generated double mutants of mouse HIF-2 α (S304M and G323E) and performed HRE-Luc assays to assess the effect of the mutations on HMP-mediated HIF-2 α inhibition.¹⁶ The HRE-Luc assays indicated that HMP mediates HIF-2 α inhibition via these two residues (Figures 4G and 4H). Next, by liquid chromatography-mass spectrometry (LC-MS), we found that the concentrations of HMP produced by *R. torques* much more than *C. hathewayi* did (Figure 4I). We also found that HMP levels were elevated after *R. torques* administration rather than *C. hathewayi* administration, both in intestinal tissue and in the feces (Figures 4J and 4K). In addition, the concentrations of HMP were at high levels in the feces of participants after TRF intervention in our clinical study and showed a negative correlation with HSI (Figures 4L and 4M). Taken together,

Figure 3. HIF-2 α -ceramide signaling mediates the beneficial effects of *R. torques* on MASLD

(A and B) Transcriptome analysis of intestinal epithelial cells by RNA-seq between *R. torques*-gavaged mice and PBS-gavaged mice. GO pathway analysis (A) and transcription factors enrichment analysis (B).
(C) Relative mRNA expressions related to *Hif2a* in intestinal epithelial cells from *R. torques*-gavaged mice and PBS-gavaged mice.
(D and E) Intestinal lipid profiles between the two groups by the application of lipidomics. PLS-DA analysis of lipid metabolites in the ileum (D) and random forest analysis showing the top 15 lipid metabolites that lead to differences in the ileal lipid profiles (E).
(F) Concentrations of ceramides in intestinal epithelial cells from *R. torques*-gavaged mice and PBS-gavaged mice.
(G–I) Representative H&E (top) and oil red O (bottom) staining of liver section (G), mRNA expression of genes related to *Hif2a* in intestinal epithelial cells (H), and ceramide concentrations of intestinal epithelial cells (I) from *Hif2a*^{fl/fl} mice or *Hif2a*^{dIE} mice treated with *R. torques* gavage or PBS gavage for 8 weeks. Scale bars, 100 μ m.
(J–L) Representative H&E (top) and oil red O (bottom) staining of liver section (J), relative mRNA expressions related to *Hif2a* (K), and the ceramide concentrations (L) of intestinal epithelial cells from C57BL/6J mice treated with LV-GFP or LV-HIF-2 α and fed with an HFD for 8 weeks. Scale bars, 100 μ m.
n = 6 per group. Data are shown as the median with first and third quartiles in box and whiskers (C, F, H, I, K, and L). *p* values were determined by two-tailed Student's *t* test (C), Mann-Whitney U tests (F), one-way ANOVA with Dunnett's T3 post hoc test (H), one-way ANOVA with Tukey post hoc test (K), and Kruskal-Wallis test with Dunn's test (I and L). In (C) and (F), **p* < 0.05 and ***p* < 0.01 versus the control group. In (H) and (I), **p* < 0.05 and ***p* < 0.01 versus the *Hif2a*^{fl/fl} group. In (K) and (L), **p* < 0.05 and ***p* < 0.01 versus the LV-GFP group and #*p* < 0.05 and ##*p* < 0.01 versus the LV-HIF-2 α group. Ctrl, control; GO, Gene Ontology; H&E, hematoxylin-eosin staining; PLS-DA, partial least squares discriminant analysis; *Rt*, *R. torques*.

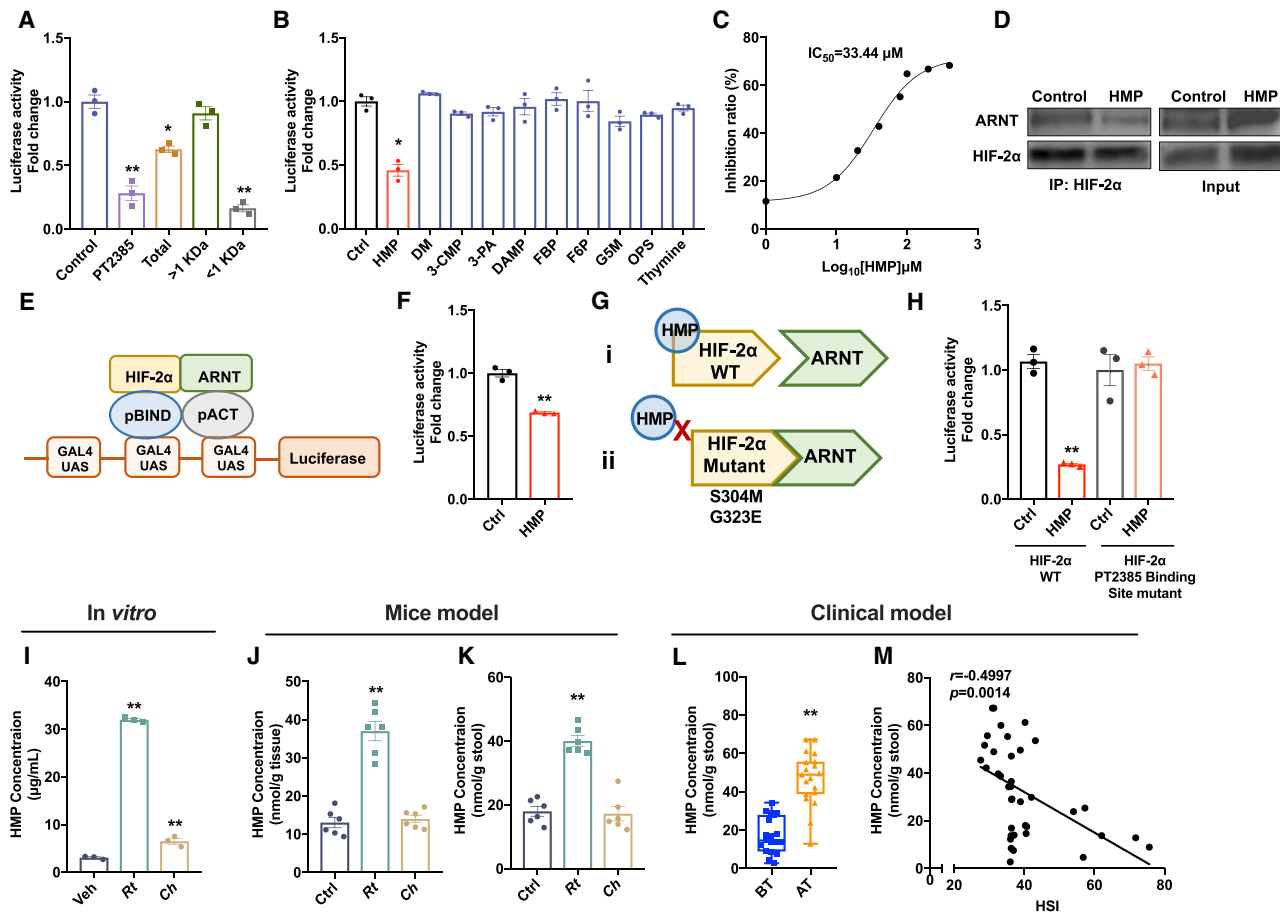


Figure 4. HMP is an endogenous inhibitor of HIF-2 α

(A) HIF-2 α luciferase activity of HEK293T cells exposed to >1 kDa fraction or <1 kDa fraction for 24 h. (B) HIF-2 α luciferase activity of HEK293T cells exposed to different metabolites of *R. torques*. (C) Inhibition curve of HMP for the suppression of HIF-2 α transcriptional activity as determined by luciferase assay. (D) Co-immunoprecipitation for ARNT and HIF-2 α in HEK293T cells treated with HMP. (E and F) Schematic (E) and experimental (F) of mammalian two-hybrid assay, showing HMP inhibits HIF-2 α -ARNT interaction. (G and H) Schematic (G) and experimental (H) representation of HMP on the mutation of PT2385-binding sites on HIF-2 α . (I) The concentration of HMP produced by *R. torques* and *C. hathewayi* *in vitro*. (J and K) The concentration of HMP in intestine tissues (J) and feces (K) from *R. torques* treatment mouse model. (L) The concentration of HMP in feces from TRF clinical model. (M) Correlative analysis of HSI and the concentration of HMP.

Data are shown as mean \pm SEM (A, B, F, and H–K) and the median with first and third quartiles in box and whiskers (L). *p* values were determined by one-way ANOVA with Dunnett’s T3 post hoc test (A, B, and I), two-tailed Student’s *t* test (F and H), one-way ANOVA with Tukey post hoc test (J and K), paired Student’s *t* test (L) and Spearman’s rank tests (M). In (A), (B), (F), and (H), **p* < 0.05 and ***p* < 0.01 versus the control group. In (I)–(K), **p* < 0.05 and ***p* < 0.01 versus the control group and ##*p* < 0.01 versus the *Rt* group. In (L), ***p* < 0.01 versus the BT group. Ctrl, control; DM, 2’-deoxyguanosine 5’-monophosphate; FBP, fructose 1,6-biphosphate; F6P, fructose 6-phosphate; G5M, guanosine 5-monophosphate; HMP, 2-hydroxy-4-methylpentanoic acid; OPS, O-phospho-serine; RT, *R. torques*; TRF, time-restricted feeding; 3-PA, 3-phosphoglyceric acid.

these findings suggest that HMP, a metabolite of *R. torques*, acts as an endogenous inhibitor of intestinal HIF-2 α in the host.

HMP produced by *rtMor* improves MASLD in mice

To further clarify whether HMP participates in the improvement of MASLD, HMP (100 mg/L) was administered to mice via drinking water on an HFD for 8 weeks. HMP improved hepatic steatosis and reduced liver weights, plasma and hepatic TG and TC levels, ALT and AST levels, as well as hepatic fatty acid transport, lipogenesis, inflammation, and fatty acid β -oxidation compared with control-treated mice (Figures S4A–S4N).

Further, administration of HMP repressed the expressions of *Neu3* and intestinal ceramide levels compared with control-treated mice (Figures S4O and S4P). In addition, 2-week HMP treatment reduced the expressions of *Neu3* and intestinal ceramide levels in *Hif2a*^{fl/fl} mice, which failed to show a further effect in the *Hif2a*^{dIE} mice (Figures S4Q and S4R).

Bacteria can synthesize HMP from 4-methyl-2-oxopentanoate (MO), an intermediate in leucine synthesis (Figure S5A).¹⁹ The bacterial enzymes exhibiting MO reductase activity have been mostly identified in *Lactobacillus*. 2-hydroxyisocaproate dehydrogenase of *Clostridioides difficile*, reported as an MO

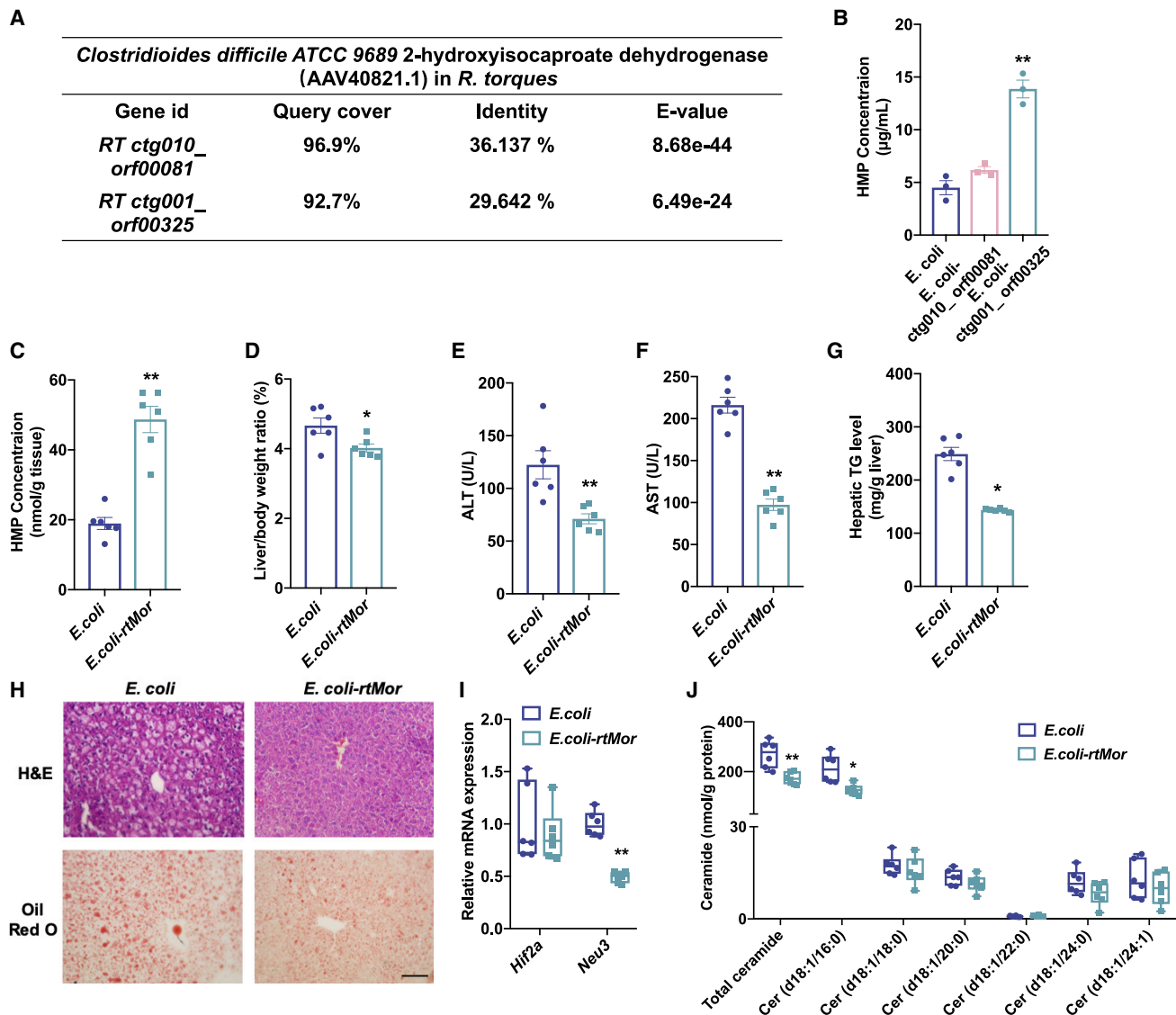


Figure 5. HMP improves HFD-induced MASLD via a HIF-2 α -ceramide axis

(A) Blast results of *Clostridioides difficile* ATCC 9689 2-hydroxyisocaproate dehydrogenase (AAV40821.1) in *R. torques*.

(B) HMP concentration of *E. coli*, *E.coli-rtMor*, and *E.coli-rtMor ctg001_orf00325*. $n = 3$.

(C–G) HMP concentration of ileum (C), liver/body weight ratio (D), ALT (E), AST (F), hepatic TG levels (G) of mice treated with *E. coli* or *E.coli-rtMor* for 8 weeks.

(H–J) Representative H&E (top) and oil red O (bottom) staining of liver section from the indicated groups of mice (H), relative mRNA expressions related to *Hif2a* (I), and the ceramide concentrations (J) of intestinal epithelial cells from mice in the indicated groups. Scale bars, 100 μ m.

Data are shown as mean \pm SEM (B–G) and the median with first and third quartiles in box and whiskers (I and J). In (C)–(J), $n = 6$ per group. p values were determined by one-way ANOVA with Tukey post hoc test (B), two-tailed Student's t test (C–G and J), and Mann-Whitney U tests (I). * $p < 0.05$ and ** $p < 0.01$ versus the *E. coli* group. ALT, alanine aminotransferase; AST, aspartate aminotransferase; H&E, hematoxylin-eosin staining; HMP, 2-hydroxy-4-methylpentanoic acid; *Rt*, *R. torques*; *rtMor*, the enzyme that catalyzes the reduction of 4-methyl-2-oxopentanoate to 2-hydroxy-4-methylpentanoic acid in *R. torques*; TG, triglyceride.

reductase to produce HMP,²⁰ was selected as a reference protein. The *R. torques* genome was screened using BLAST to find sequences encoding possible *RT ctg010_orf00081*, *RT ctg001_orf00325* (Figure 5A). As a result, the protein encoded by *RT ctg001_orf00325* is able to catalyze the reduction of MO to form HMP (Figures 5B and S5B), and thus we named the enzyme *rtMor*.

To further clarify the effect of *rtMor* *in vivo*, we generated heterologous expression of *rtMor* in *Escherichia coli* BL21 (*E. coli-*

rtMor). We then gavaged mice with *E. coli-rtMor* and found that intestinal concentrations of HMP were higher compared with the control mice (Figure 5C). Administration of *E. coli-rtMor* substantially resulted in a reduction in hepatic lipid droplets, which was reflected by lower plasma and hepatic TG and TC levels, ALT and AST levels, and hepatic fatty acid metabolism pathway and inflammation (Figures 5D–5H and S5C–S5J). Likewise, *E. coli-rtMor* treatment decreased the mRNA expression of *Neu3* and intestinal ceramide levels (Figures 5I and 5J). These

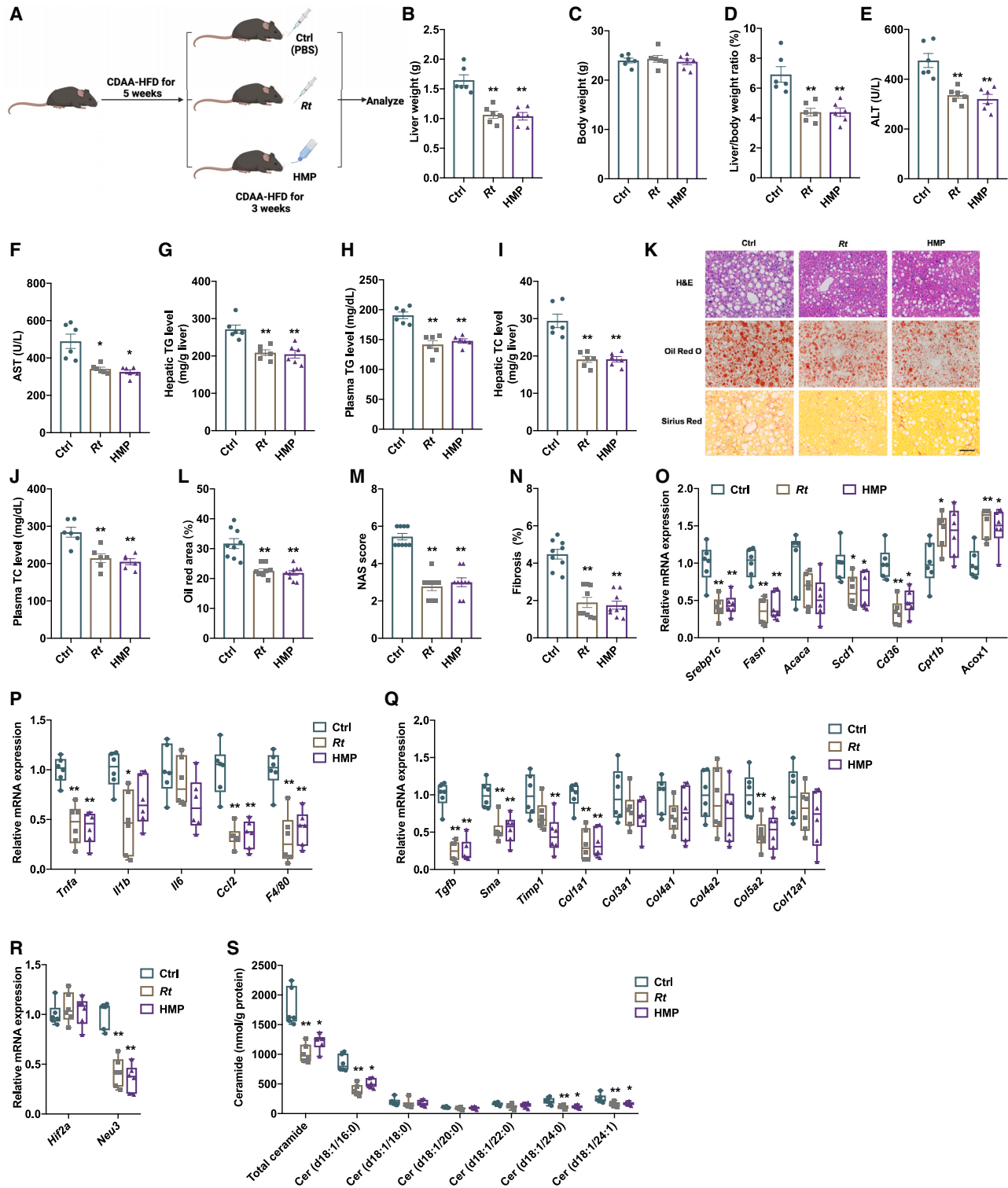


Figure 6. Administration of *R. torques* or HMP improves MASH in mice

(A) The experimental scheme for *R. torques* and HMP therapy effect of MASH. Mice were treated by CDAA-HFD for 5 weeks, when appreciable MASH was established. Then, the mice were treated by PBS (control), *R. torques*, or HMP-containing water for another 3 weeks.

(B–J) Liver weights (B), body weights (C), liver/body weight ratio (D), ALT (E), AST (F), hepatic (G) and plasma TG (H), hepatic (I), and plasma TC (J) of mice were treated with *R. torques* or HMP, combined with a CDAA-HFD diet, for 8 weeks.

(legend continued on next page)

results suggest that the supplementation of HMP protects against MASLD in a manner dependent on the activity of the intestinal HIF-2 α -ceramide axis.

***R. torques* colonization or oral HMP supplementation improves MASH**

MASH, the progressive form of MASLD, has rapidly become a leading etiology underlying many cases of HCC.²¹ To determine the role of *R. torques* and HMP in MASH progression, 8-week-old male C57BL/6J mice were treated by choline-deficient amino acid-defined and HFD (CDAA-HFD) for 8 weeks, accompanied by PBS (control), *R. torques*, or HMP water (Figure S6A). No obvious change in body weights was observed among the groups, while the liver weights, liver/body weight ratio, ALT levels, AST levels, and TG and TC levels of *R. torques* or HMP-treated mice were reduced compared with those of the control group (Figures S6B–S6J). The protective effects of *R. torques* and HMP on hepatic steatosis, inflammation, and fibrosis can be observed in liver histochemistry and qPCR results (Figures S6K–S6Q). *R. torques* or HMP treatment repressed the expressions of *Neu3* and intestinal ceramide levels (Figures S6R and S6S).

To further validate the therapeutic effect of *R. torques* and HMP on MASH, 8-week-old male C57BL/6J mice were treated by CDAA-HFD for 5 weeks when appreciable MASH was established. Then, we treated the mice with PBS (control), *R. torques*, or HMP-containing water for another 3 weeks (Figure 6A). No obvious change in body weights was observed among the groups, while the liver weights, liver/body weight ratio, serum levels of ALT and AST, and TG and TC levels of *R. torques* or HMP-treated mice were reduced compared with those of the control group (Figures 6B–6J). On the basis of H&E, oil red O, and Sirius Red staining, we found that *R. torques* or HMP supplementation slowed down the progression of MASH, as indicated by less severe hepatic steatosis, inflammation, and fibrosis (Figures 6K–6N). Furthermore, the relative expression of mRNAs involved in hepatic lipid metabolism, proinflammatory cytokine production, and collagen synthesis was reduced by *R. torques* or HMP treatment (Figures 6O–6Q). Further, *R. torques* or HMP treatment repressed the expressions of *Neu3* and intestinal ceramide levels (Figures 6R and 6S). Thus, *R. torques* and HMP administration are both effective means to prevent and treat fatty liver.

To confirm whether modulation of the ceramide profiles accounts for the dependency of the beneficial effects of *R. torques* on MASLD/MASH on the HIF-2 α -ceramide pathway, we administered ceramide (d18:1/16:0) by intraperitoneal (i.p.) injection every other day. The protective effects

on hepatic steatosis, inflammation, and fibrosis resulting from *R. torques* administration were reversed by ceramide (d18:1/16:0) administration (Figures S7A–S7S). In conclusion, *R. torques*-induced inhibition of the intestinal HIF-2 α -ceramide axis mitigated MASLD progression by decreasing intestinal ceramide production.

***R. torques*-HMP participates in intermittent fasting-mediated improvements in MASLD**

An intermittent fasting 5:2 diet (5A2F), which refers to 5 days of *ad libitum* eating and 2 days of starvation per week, is another popular dietary intervention.^{22,23} We also enrolled 15 participants with MASLD for a 4-week 5A2F intervention (Table S2). After the 4-week 5A2F intervention, the indicators of liver damage (HSI, ALT, AST, ALP, and GGT) and TG levels were obviously decreased, accompanied by a decreased BMI (Figures 7A–7G). The α -diversity was slightly increased after 5A2F intervention; meanwhile, the PCoA showed no significant difference (Figures 7H–7K). By LEfSe analysis, we found that *R. torques* levels were significantly increased after 5A2F (Figure 7L). We found that the abundance of *R. torques* showed a striking negative correlation with HSI (Figure 7M). The levels of HMP increased significantly after 5A2F (Figure 7N). In addition, the levels of HMP exhibited a negative correlation with HSI (Figure 7O). These findings corroborated that *R. torques*-HMP may participate in the process of 5A2F-mediated improvement of MASLD.

DISCUSSION

Most studies investigating the effects of TRF have mainly focused on body weight and glucose regulation, revealing the analogous effects of weight reduction and insulin sensitivity observed in various TRF regimes. However, only a few clinical studies have assessed the role of TRF in patients with MASLD, but they failed to identify the intrinsic mechanisms involved.^{24,25} In this study, we revealed that *R. torques* and its metabolite HMP improve MASLD/MASH, which is dependent on the intestinal HIF-2 α -ceramide axis, a novel mechanism for how TRF directly affects liver steatosis.

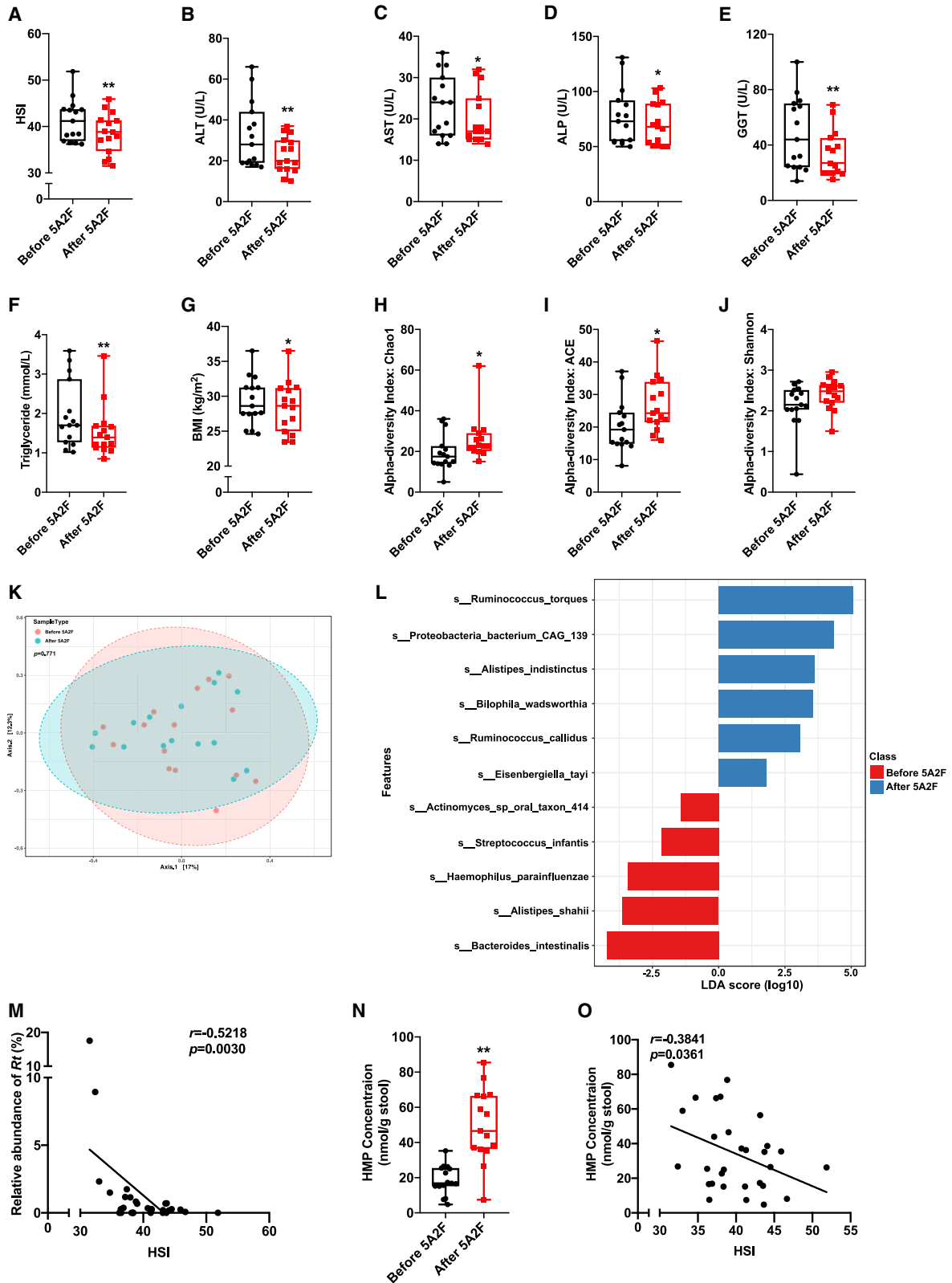
Le Roy et al. transplanted the gut microbiota of obese mice with or without liver steatosis into germ free (GF) mice and found that mice that received feces from steatotic mice showed higher liver TG content, as well as higher expression of genes involved in lipid absorption and *de novo* lipogenesis, without a significant difference in body weight between the two groups.²⁶ These results suggest that the gut microbiota promotes the development of MASLD independently of obesity. Consistent with their

(K) Representative H&E staining (top), oil red O staining (middle), and Sirius Red staining (bottom) of liver section from the indicated groups of mice. Scale bars, 100 μ m.

(L–N) Histology scores of oil red O (L), NAFLD activity (M), and fibrosis (N).

(O–Q) Relative mRNA expressions of the indicated genes related to fatty acid transport and lipogenesis-related genes, fatty acid β -oxidation-related genes (O), inflammatory cytokine (P), and fibrosis (Q).

(R and S) Relative mRNA expressions related to *Hif2a* (R) and the ceramide concentrations (S) of intestinal epithelial cells from mice in the indicated groups. $n = 6$ per group. Data are shown as mean \pm SEM (B–J and L–N) and the median with first and third quartiles in box and whiskers (O–S). p values were determined by one-way ANOVA with Tukey post hoc test (B–E, G, H, J, and P), one-way ANOVA with Dunnett's T3 post hoc test (F, I, and L), and Kruskal-Wallis test with Dunn's test (M, N, O, and Q–S). * $p < 0.05$ and ** $p < 0.01$ versus the Ctrl group. ALT, alanine aminotransferase; AST, aspartate aminotransferase; Cer, ceramide; Ctrl, control; H&E, hematoxylin-eosin staining; HMP, 2-hydroxy-4-methylpentanoic acid; NAS, NAFLD activity score; *Rt*, *R. torques*; TC, total cholesterol; TG, triglyceride.



(legend on next page)

results, we found that 2-week *R. torques* treatment improved hepatic TG and ceramide levels before the onset of body weight change.

Ruminococcus genus was found to be closely associated with obesity, and the abundance of *R. torques* is increased in a weight loss group.^{27,28} Moreover, recent research has identified *R. torques* as one of the most predictive bacterial species for obesity status.²⁹ Our groundbreaking study goes beyond these findings by providing the first experimental evidence of a probiotic effect of *R. torques* in MASLD/MASH, with detailed molecular insights into the underlying mechanism at play. Despite the ameliorative effect of *R. torques* on MASLD/MASH, we did not observe a significant difference in the abundance of *R. torques* between patients with MASLD and healthy volunteers.³⁰ Although *R. torques* remains unchanged in patients with MASLD in these studies, supplementation with *R. torques* has an important role in the treatment of metabolic disorders based on our findings of the role of *R. torque* in improving MASLD.

Interestingly, metformin treatment increases the abundance of *R. torques*, which correlated with lower fasting insulin.³¹ Our previous study found that ablation of intestinal HIF-2 α down-regulates gut lactic acid concentrations, which led to a reduction in *Bacteroides vulgatus* (*B. vulgatus*). We also found that the abundance of *R. torques* was negatively correlated with that of *B. vulgatus*, thus activated HIF-2 α -lactic acid axis could indirectly reduce *R. torques* abundance.³² In this study, we found that TRF enriches *R. torques* abundance, thereby increasing HMP production and reducing ceramide-mediated hepatic steatosis. Consistently, one 3-month TRF trial showed a similar increase in *R. torque* abundance.³³ Conversely, the metagenome result of another clinical trial showed that *R. torques* abundance remained unchanged following a 12-week period of the 5:2 diet.³⁴ This discrepancy between these results and our own may be attributed to discrepancies in participant diets, lifestyles, or geographic regions.³⁵ Thus, a future study is needed to fully understand the deeper mechanism by which TRF may enrich *R. torques* levels in gut.

We discovered that *R. torques*-derived metabolite HMP acts as a TRF mimic that can inhibit intestinal HIF-2 α -ceramide signaling to attenuate diet-induced liver steatosis. HMP, which is derived from L-leucine, was found long ago to be generated by anaerobic bacteria. However, the reductase that catalyzes the formation of HMP from 4-methyl-2-oxopentanoic acid as an intermediate has not yet been identified in *Ruminococcus*.³⁶ Although many bacteria, especially *Lactobacillus*,³⁷ can produce HMP, TRF-enriched *R. torques* is the most significantly altered HMP-producing bacteria, and their elevated HMP levels can improve MASLD by inhibiting the intestinal HIF-2 α -ceramide

axis. Currently, HMP is not reported to be associated with physiological metabolism, while our study has demonstrated the ameliorative effect of HMP on MASLD/MASH as a potential therapeutic agent. Indeed, bioengineering of bacteria to produce HMP may provide a “bugs for drugs” approach to ameliorate this difficult-to-treat condition.

In conclusion, we determined that a TRF regime promotes the growth of *R. torques*, contributing to improvements in MASLD/MASH via an HMP-HIF-2 α -ceramide axis. These findings deepen our understanding of the mechanisms by which intestinal commensal bacteria regulate the development of host metabolic diseases while providing novel strategies to mimic a fasting dietary regime that may be too difficult for most people to adhere to consistently.

Limitations of the study

The use of antibiotics is the common method for studying the gut microbiota. There are different reports regarding the impact of antibiotics on MASLD. Some studies reported that use of antibiotics improved MASLD.^{38–40} By contrast, Schneider et al. reported antibiotic treatment aggravated murine methionine-choline deficient (MCD) induced MASH,⁴¹ Du et al. reported Abx treatment elevated hepatic TG content and serum ALT levels in HFD-fed mice,⁴² and Yu et al. reported antibiotic azithromycin-induced steatosis in HFD-fed mice.⁴³ In addition, others reported that antibiotic treatment does not alter serum ALT and AST levels in HFD-fed mice.^{44,45} In our study, we did not observe a difference between the control and control+Abx groups. In view of the different types of antibiotics between different studies, we think the type and spectrum of the Abx, the background of the mice, or the feeding environment may result in different gut microbiota composition and different outcomes. This also indicates that the role of broad-spectrum clearance of all bacterial communities in the progression of MASH is unclear, and it is thus necessary to clarify the function of characteristic bacteria. Future interventions targeting the function of characteristic bacteria have better prospects for future clinical translation.

We have clarified the important role of *R. torques* and HMP in the progression of MASLD/MASH, but unfortunately, *R. torques* is difficult to genetically manipulate. But in spite of a lack of genetical validation of *R. torques* via a loss-of-function approach, we did use a gain-of-function approach by generating heterologous expression of *rtMor* in *E. coli* BL21 to validate the vital role of HMP in ameliorating MASLD/MASH progression.

As we discussed above, different intermittent fasting studies showed different gut microbiota change, which may result from different diets or different geographic regions of the cohorts

Figure 7. 5A2F intervention increases *R. torques* and HMP levels

(A–G) HSI (A), ALT (B), AST (C), ALP (D), GGT (E), triglyceride (F), and BMI (G) of participants with MASLD before and after 5A2F intervention.

(H–J) α -diversity of the gut microbiota of participants before and after TRF intervention, as indicated by the Chao1 (H), ACE (I), and Shannon (J) indices.

(K) β -Diversity of participants before and after 5A2F intervention.

(L) The LEfSe was conducted to identify the differentially abundant bacteria among the baseline and 5A2F groups.

(M) Correlative analysis of the relative abundance of *R. torques* and HSI.

(N) The concentration of HMP in feces of participants before and after 5A2F.

(O) Correlative analysis of the concentration of HMP and HSI.

n = 15 per group. Data are shown as the median with first and third quartiles in box and whiskers (A–J and N). *p* values were determined by paired *t* test (A, C, E, G, H, I, and N), Wilcoxon's sign rank test (B, D, F, and J), Spearman's rank tests (M and O), and PERMANOVA based on Bray-Curtis index (K). **p* < 0.05 and ***p* < 0.01 versus the before 5A2F group. ALT, alanine aminotransferase; ALP, alkaline phosphatase; AST, aspartate aminotransferase; BMI, body mass index; GGT, gamma-glutamyltransferase; HSI, hepatorenal steatosis index; HMP, 2-hydroxy-4-methylpentanoic acid; TG, triglyceride; 5A2F, 5:2 intermittent fasting.

studied. We propose that large and multi-centered clinical trials should be conducted to further confirm the benefits of TRF for MASLD/MASH progression.

STAR★METHODS

Detailed methods are provided in the online version of this paper and include the following:

- KEY RESOURCES TABLE
- RESOURCE AVAILABILITY
 - Lead contact
 - Materials availability
 - Data and code availability
- EXPERIMENTAL MODEL AND SUBJECT DETAILS
 - Human subjects and sample collection
 - Mice and treatments
 - Microbe strains and culture
- METHOD DETAILS
 - DNA extraction
 - Metagenomics sequencing
 - Biochemical assays
 - Histological analysis
 - Real-time quantitative PCR analysis and RNA-seq profiling
 - Metabolomics analysis
 - Luciferase reporter gene assays
 - Co-immunoprecipitation and western blotting
 - HMP level measurements
- QUANTIFICATION AND STATISTICAL ANALYSIS

SUPPLEMENTAL INFORMATION

Supplemental information can be found online at <https://doi.org/10.1016/j.cmet.2024.07.004>.

ACKNOWLEDGMENTS

C.J. acknowledges support from the Tencent Foundation through the Xplorer Prize. We thank Shuang-jiang Liu (State Key Laboratory of Microbial Resources, Institute of Microbiology, Chinese Academy of Sciences) for his help in obtaining *Eubacterium rectale*. Funding: this work was supported by the National Natural Science Foundation of the P.R. of China (nos. 31925021, 82130022, 82022028, 82171627, 82288102, 81972702, 82273104, 91959110, 62173005, and 82370848), the National Key Research and Development Program of China (2018YFA0800700 and 2022YFA0806400), and the Peking University Clinical Scientist Training Program Project (BMU2023PYJH021).

AUTHOR CONTRIBUTIONS

C.J., Y.P., W.F., Z.Z., and G.W. conceptualized and designed the study. Y.Z., X.W., J. Lin, K.W., Q.N., C.Y., L.S., Y. Ma, and R.Q. performed the experiments and analyzed the data. Y. Mao, X.Z., H.L., P.X., and D.Z. provided strains. J. Liu and G.W. collected clinical samples. Y.Z., X.W., J. Lin, and C.J. wrote the manuscript. Y.Z., X.W., J. Lin, and J. Liu contributed equally to this work. All authors edited the manuscript and approved the final manuscript.

DECLARATION OF INTERESTS

Y. Mao and X.Z. are employees of the Mengniu Institute of Nutrition Science. This study is supported in part by a research fund from the Mengniu Institute of Nutrition Science.

Received: May 5, 2023
Revised: January 24, 2024
Accepted: July 5, 2024
Published: July 29, 2024

REFERENCES

1. Rinella, M.E., Lazarus, J.V., Ratzliff, V., Francque, S.M., Sanyal, A.J., Kanwal, F., Romero, D., Abdelmalek, M.F., Anstee, Q.M., Arab, J.P., et al. (2023). A multisociety Delphi consensus statement on new fatty liver disease nomenclature. *Hepatology* 78, 1966–1986. <https://doi.org/10.1097/HEP.0000000000000520>.
2. Powell, E.E., Wong, V.W.S., and Rinella, M. (2021). Non-alcoholic fatty liver disease. *Lancet* 397, 2212–2224. [https://doi.org/10.1016/S0140-6736\(20\)32511-3](https://doi.org/10.1016/S0140-6736(20)32511-3).
3. Samuel, V.T., and Shulman, G.I. (2018). Nonalcoholic Fatty Liver Disease as a Nexus of Metabolic and Hepatic Diseases. *Cell Metab.* 27, 22–41. <https://doi.org/10.1016/j.cmet.2017.08.002>.
4. Younossi, Z., Tacke, F., Arrese, M., Chander Sharma, B., Mostafa, I., Bugianesi, E., Wai-Sun Wong, V., Yilmaz, Y., George, J., Fan, J., and Vos, M.B. (2019). Global Perspectives on Nonalcoholic Fatty Liver Disease and Nonalcoholic Steatohepatitis. *Hepatology* 69, 2672–2682. <https://doi.org/10.1002/hep.30251>.
5. Di Francesco, A., Di Germanio, C., Bernier, M., and de Cabo, R. (2018). A time to fast. *Science* 362, 770–775. <https://doi.org/10.1126/science.aau2095>.
6. Wilkinson, M.J., Manoogian, E.N.C., Zadorian, A., Lo, H., Fakhouri, S., Shoghi, A., Wang, X., Fleischer, J.G., Navlakha, S., Panda, S., and Taub, P.R. (2020). Ten-Hour Time-Restricted Eating Reduces Weight, Blood Pressure, and Atherogenic Lipids in Patients with Metabolic Syndrome. *Cell Metab.* 31, 92–104.e5. <https://doi.org/10.1016/j.cmet.2019.11.004>.
7. Sun, S., Hanzawa, F., Umeki, M., Ikeda, S., Mochizuki, S., and Oda, H. (2018). Time-restricted feeding suppresses excess sucrose-induced plasma and liver lipid accumulation in rats. *PLoS One* 13, e0201261. <https://doi.org/10.1371/journal.pone.0201261>.
8. Wei, X., Lin, B., Huang, Y., Yang, S., Huang, C., Shi, L., Liu, D., Zhang, P., Lin, J., Xu, B., et al. (2023). Effects of Time-Restricted Eating on Nonalcoholic Fatty Liver Disease: The TREATY-FLD Randomized Clinical Trial. *JAMA Netw. Open* 6, e233513. <https://doi.org/10.1001/jamanetworkopen.2023.3513>.
9. Demehri, F.R., Barrett, M., and Teitelbaum, D.H. (2015). Changes to the Intestinal Microbiome With Parenteral Nutrition: Review of a Murine Model and Potential Clinical Implications. *Nutr. Clin. Pract.* 30, 798–806. <https://doi.org/10.1177/0884533615609904>.
10. Li, G., Xie, C., Lu, S., Nichols, R.G., Tian, Y., Li, L., Patel, D., Ma, Y., Brocker, C.N., Yan, T., et al. (2017). Intermittent Fasting Promotes White Adipose Browning and Decreases Obesity by Shaping the Gut Microbiota. *Cell Metab.* 26, 801. <https://doi.org/10.1016/j.cmet.2017.10.007>.
11. Zarrinpar, A., Chaix, A., Yooseph, S., and Panda, S. (2014). Diet and feeding pattern affect the diurnal dynamics of the gut microbiome. *Cell Metab.* 20, 1006–1017. <https://doi.org/10.1016/j.cmet.2014.11.008>.
12. Chu, H., Duan, Y., Yang, L., and Schnabl, B. (2019). Small metabolites, possible big changes: a microbiota-centered view of non-alcoholic fatty liver disease. *Gut* 68, 359–370. <https://doi.org/10.1136/gutjnl-2018-316307>.
13. Ramakrishnan, S.K., and Shah, Y.M. (2016). Role of Intestinal HIF-2 α in Health and Disease. *Annu. Rev. Physiol.* 78, 301–325. <https://doi.org/10.1146/annurev-physiol-021115-105202>.
14. Xie, C., Yagai, T., Luo, Y., Liang, X., Chen, T., Wang, Q., Sun, D., Zhao, J., Ramakrishnan, S.K., Sun, L., et al. (2017). Activation of intestinal hypoxia-inducible factor 2 α during obesity contributes to hepatic steatosis. *Nat. Med.* 23, 1298–1308. <https://doi.org/10.1038/nm.4412>.
15. Canfora, E.E., Meex, R.C.R., Venema, K., and Blaak, E.E. (2019). Gut microbial metabolites in obesity, NAFLD and T2DM. *Nat. Rev. Endocrinol.* 15, 261–273. <https://doi.org/10.1038/s41574-019-0156-z>.
16. Das, N.K., Schwartz, A.J., Barthel, G., Inohara, N., Liu, Q., Sankar, A., Hill, D.R., Ma, X., Lamberg, O., Schnitzlein, M.K., et al. (2020). Microbial Metabolite Signaling Is Required for Systemic Iron

- Homeostasis. *Cell Metab.* 31, 115–130.e6. <https://doi.org/10.1016/j.cmet.2019.10.005>.
17. Li, Q., Hu, W., Liu, W.X., Zhao, L.Y., Huang, D., Liu, X.D., Chan, H., Zhang, Y., Zeng, J.D., Coker, O.O., et al. (2021). *Streptococcus thermophilus* Inhibits Colorectal Tumorigenesis Through Secreting β -Galactosidase. *Gastroenterology* 160, 1179–1193.e14. <https://doi.org/10.1053/j.gastro.2020.09.003>.
 18. Han, S., Van Treuren, W., Fischer, C.R., Merrill, B.D., DeFelice, B.C., Sanchez, J.M., Higginbottom, S.K., Guthrie, L., Fall, L.A., Dodd, D., et al. (2021). A metabolomics pipeline for the mechanistic interrogation of the gut microbiome. *Nature* 595, 415–420. <https://doi.org/10.1038/s41586-021-03707-9>.
 19. Shimizu, M., Yamamoto, T., Okabe, N., Sakai, K., Koide, E., Miyachi, Y., Kurimoto, M., Mochizuki, M., Yoshino-Yasuda, S., Mitsui, S., et al. (2016). Novel 4-methyl-2-oxopentanoate reductase involved in synthesis of the Japanese sake flavor, ethyl leucate. *Appl. Microbiol. Biotechnol.* 100, 3137–3145. <https://doi.org/10.1007/s00253-015-7182-0>.
 20. Kim, J., Darley, D., Selmer, T., and Buckel, W. (2006). Characterization of (R)-2-hydroxyisocaproate dehydrogenase and a family III coenzyme A transferase involved in reduction of L-leucine to isocaproate by *Clostridium difficile*. *Appl. Environ. Microbiol.* 72, 6062–6069. <https://doi.org/10.1128/AEM.00772-06>.
 21. Anstee, Q.M., Reeves, H.L., Kotsiliti, E., Govaere, O., and Heikenwalder, M. (2019). From NASH to HCC: current concepts and future challenges. *Nat. Rev. Gastroenterol. Hepatol.* 16, 411–428. <https://doi.org/10.1038/s41575-019-0145-7>.
 22. Carter, S., Clifton, P.M., and Keogh, J.B. (2018). Effect of Intermittent Compared With Continuous Energy Restricted Diet on Glycemic Control in Patients With Type 2 Diabetes: A Randomized Noninferiority Trial. *JAMA Netw. Open* 1, e180756. <https://doi.org/10.1001/jamanetworkopen.2018.0756>.
 23. Varady, K.A., Cienfuegos, S., Ezpeleta, M., and Gabel, K. (2022). Clinical application of intermittent fasting for weight loss: progress and future directions. *Nat. Rev. Endocrinol.* 18, 309–321. <https://doi.org/10.1038/s41574-022-00638-x>.
 24. Cai, H., Qin, Y.L., Shi, Z.Y., Chen, J.H., Zeng, M.J., Zhou, W., Chen, R.Q., and Chen, Z.Y. (2019). Effects of alternate-day fasting on body weight and dyslipidaemia in patients with non-alcoholic fatty liver disease: a randomised controlled trial. *BMC Gastroenterol.* 19, 219. <https://doi.org/10.1186/s12876-019-1132-8>.
 25. Mari, A., Khoury, T., Baker, M., Said Ahmad, H., Abu Baker, F., and Mahamid, M. (2021). The Impact of Ramadan Fasting on Fatty Liver Disease Severity: A Retrospective Case Control Study from Israel. *Isr. Med. Assoc. J.* 23, 94–98.
 26. Le Roy, T., Llopis, M., Lepage, P., Bruneau, A., Rabot, S., Bevilacqua, C., Martin, P., Philippe, C., Walker, F., Bado, A., et al. (2013). Intestinal microbiota determines development of non-alcoholic fatty liver disease in mice. *Gut* 62, 1787–1794. <https://doi.org/10.1136/gutjnl-2012-303816>.
 27. Chakraborti, C.K. (2015). New-found link between microbiota and obesity. *World J. Gastrointest. Pathophysiol.* 6, 110–119. <https://doi.org/10.4291/wjgp.v6.i4.110>.
 28. Oba, P.M., Kelly, J., Kostiuik, D., and Swanson, K.S. (2023). Effects of weight loss and feeding specially formulated diets on the body composition, blood metabolite profiles, voluntary physical activity, and fecal metabolites and microbiota of obese dogs. *J. Anim. Sci.* 107, skad073. <https://doi.org/10.1093/jas/skad073>.
 29. Meijnikman, A.S., Aydin, O., Prodan, A., Tremaroli, V., Herrema, H., Levin, E., Acherman, Y., Bruin, S., Gerdes, V.E., Backhed, F., et al. (2020). Distinct differences in gut microbial composition and functional potential from lean to morbidly obese subjects. *J. Intern. Med.* 288, 699–710. <https://doi.org/10.1111/joim.13137>.
 30. Hoyles, L., Fernández-Real, J.M., Federici, M., Serino, M., Abbott, J., Charpentier, J., Heymes, C., Luque, J.L., Anthony, E., Barton, R.H., et al. (2018). Molecular phenomics and metagenomics of hepatic steatosis in non-diabetic obese women. *Nat. Med.* 24, 1070–1080. <https://doi.org/10.1038/s41591-018-0061-3>.
 31. Mueller, N.T., Differding, M.K., Zhang, M., Maruthur, N.M., Juraschek, S.P., Miller, E.R., 3rd, Appel, L.J., and Yeh, H.C. (2021). Metformin Affects Gut Microbiome Composition and Function and Circulating Short-Chain Fatty Acids: A Randomized Trial. *Diabetes Care* 44, 1462–1471. <https://doi.org/10.2337/dc20-2257>.
 32. Wu, Q., Liang, X., Wang, K., Lin, J., Wang, X., Wang, P., Zhang, Y., Nie, Q., Liu, H., Zhang, Z., et al. (2021). Intestinal hypoxia-inducible factor 2 α regulates lactate levels to shape the gut microbiome and alter thermogenesis. *Cell Metab.* 33, 1988–2003.e7. <https://doi.org/10.1016/j.cmet.2021.07.007>.
 33. Stanislawski, M.A., Frank, D.N., Borengasser, S.J., Ostendorf, D.M., Ir, D., Jambal, P., Bing, K., Wayland, L., Siebert, J.C., Bessesen, D.H., et al. (2021). The Gut Microbiota during a Behavioral Weight Loss Intervention. *Nutrients* 13, 3248. <https://doi.org/10.3390/nu13093248>.
 34. Tay, A., Pringle, H., Penning, E., Plank, L.D., and Murphy, R. (2020). PROFAST: A Randomized Trial Assessing the Effects of Intermittent Fasting and Probiotic among People with Prediabetes. *Nutrients* 12, 3530. <https://doi.org/10.3390/nu12113530>.
 35. Parizadeh, M., and Arrieta, M.C. (2023). The global human gut microbiome: genes, lifestyles, and diet. *Trends Mol. Med.* 29, 789–801. <https://doi.org/10.1016/j.molmed.2023.07.002>.
 36. Carlier, J.P., and Sellier, N. (1989). Gas chromatographic-mass spectral studies after methylation of metabolites produced by some anaerobic bacteria in spent media. *J. Chromatogr.* 493, 257–273. [https://doi.org/10.1016/s0378-4347\(00\)82733-4](https://doi.org/10.1016/s0378-4347(00)82733-4).
 37. Niyibizi, C., and Eyre, D.R. (1994). Structural characteristics of cross-linking sites in type V collagen of bone. Chain specificities and heterotypic links to type I collagen. *Eur. J. Biochem.* 224, 943–950. <https://doi.org/10.1111/j.1432-1033.1994.00943.x>.
 38. Hu, J., Luo, H., Jiang, Y., and Chen, P. (2017). Dietary capsaicin and antibiotics act synergistically to reduce non-alcoholic fatty liver disease induced by high fat diet in mice. *Oncotarget* 8, 38161–38175. <https://doi.org/10.18632/oncotarget.16975>.
 39. Zhao, M., Jiang, Z., Cai, H., Li, Y., Mo, Q., Deng, L., Zhong, H., Liu, T., Zhang, H., Kang, J.X., and Feng, F. (2020). Modulation of the Gut Microbiota during High-Dose Glycerol Monolaurate-Mediated Amelioration of Obesity in Mice Fed a High-Fat Diet. *mBio* 11, e00190-20. <https://doi.org/10.1128/mBio.00190-20>.
 40. Ding, Q., Guo, R., Pei, L., Lai, S., Li, J., Yin, Y., Xu, T., Yang, W., Song, Q., Han, Q., et al. (2022). N-Acetylcysteine alleviates high fat diet-induced hepatic steatosis and liver injury via regulating the intestinal microecology in mice. *Food Funct.* 13, 3368–3380. <https://doi.org/10.1039/d1fo03952k>.
 41. Schneider, K.M., Mohs, A., Kilic, K., Candels, L.S., Elfers, C., Bennek, E., Schneider, L.B., Heymann, F., Gassler, N., Penders, J., and Trautwein, C. (2019). Intestinal Microbiota Protects against MCD Diet-Induced Steatohepatitis. *Int. J. Mol. Sci.* 20, 308. <https://doi.org/10.3390/ijms20020308>.
 42. Du, J.J., Zhang, P.W., Luo, J., Shen, L.Y., Zhang, S.H., Gu, H., He, J., Wang, L.H., Zhao, X., Gan, M.L., et al. (2021). Dietary betaine prevents obesity through gut microbiota-driven microRNA-378a family. *Gut Microbes* 13, 1–19. <https://doi.org/10.1080/19490976.2020.1862612>.
 43. Yu, J., Chen, X., Zhang, Y., Cui, X., Zhang, Z., Guo, W., Wang, D., Huang, S., Chen, Y., Hu, Y., et al. (2022). Antibiotic Azithromycin inhibits brown/beige fat functionality and promotes obesity in human and rodents. *Theranostics* 12, 1187–1203. <https://doi.org/10.7150/thno.63067>.
 44. Liu, J., Sun, J., Yu, J., Chen, H., Zhang, D., Zhang, T., Ma, Y., Zou, C., Zhang, Z., Ma, L., and Yu, X. (2023). Gut microbiome determines therapeutic effects of OCA on NAFLD by modulating bile acid metabolism.

- NPJ Biofilms Microbiomes 9, 29. <https://doi.org/10.1038/s41522-023-00399-z>.
45. Zhou, Y.L., Zheng, T.Y., Chen, H.T., Li, Y.Q., Huang, H.L., Chen, W.J., Du, Y.L., He, J., Li, Y.Y., Cao, J., et al. (2018). Microbial Intervention as a Novel Target in Treatment of Non-Alcoholic Fatty Liver Disease Progression. *Cell. Physiol. Biochem.* 51, 2123–2135. <https://doi.org/10.1159/000495830>.
46. Bauer, P.V., Duca, F.A., Waise, T.M.Z., Dranse, H.J., Rasmussen, B.A., Puri, A., Rasti, M., O'Brien, C.A., and Lam, T.K.T. (2018). *Lactobacillus gasseri* in the Upper Small Intestine Impacts an ACSL3-Dependent Fatty Acid-Sensing Pathway Regulating Whole-Body Glucose Homeostasis. *Cell Metab.* 27, 572–587.e6. <https://doi.org/10.1016/j.cmet.2018.01.013>.
47. Sun, L., Xie, C., Wang, G., Wu, Y., Wu, Q., Wang, X., Liu, J., Deng, Y., Xia, J., Chen, B., et al. (2018). Gut microbiota and intestinal FXR mediate the clinical benefits of metformin. *Nat. Med.* 24, 1919–1929. <https://doi.org/10.1038/s41591-018-0222-4>.
48. Chen, B., Sun, L., Zeng, G., Shen, Z., Wang, K., Yin, L., Xu, F., Wang, P., Ding, Y., Nie, Q., et al. (2022). Gut bacteria alleviate smoking-related NASH by degrading gut nicotine. *Nature* 610, 562–568. <https://doi.org/10.1038/s41586-022-05299-4>.

STAR★METHODS

KEY RESOURCES TABLE

REAGENT or RESOURCE	SOURCE	IDENTIFIER
Antibodies		
Anti-HIF2a rabbit polyclonal antibody	Novus	Cat# NB100-122; RRID: AB_10002593
Anti-ARNT mouse polyclonal antibody	Santa Cruz	Cat# sc-55526; RRID: AB_673397
HRP Goat Anti-Rabbit IgG (H+L)	ABclonal	Cat#AS014; RRID: AB_2769854
HRP Goat Anti-Mouse IgG (H+L)	ABclonal	Cat#AS003; RRID: AB_2769851
Bacterial and virus strains		
<i>R. torques</i>	BNCC	bncc360706
<i>E. coli</i> BL21	Beijing Zoman Biotechnology Co., Ltd	N/A
Chemicals, peptides, and recombinant proteins		
Trizol	Thermo Fisher	Cat#15596018
Methanol	Beijing Chemical Works	Cat#B0301005
Isopropanol	Beijing Chemical Works	Cat#B0301007
Ethanol	Beijing Chemical Works	Cat#B0301002
RIPA buffer	Beyotime Biotechnology	Cat#P0013C
Vancomycin	Sigma-Aldrich	Cat#V2002
Ampicillin	Sigma-Aldrich	Cat#BP021
Kanamycin	Sigma-Aldrich	Cat#D403
Metronidazole	Sigma-Aldrich	Cat#M1547
2-hydroxy-4-methylpentanoic acid	Acmecc	Cat#S94250
2' -deoxyguanosine 5'-monophosphate	Sigma-Aldrich	Cat#85222
3-CMP	Chromadex	Cat#ASB-00003997
3-phosphoglyceric acid	Acmecc	Cat#D74380
DAMP	Acmecc	Cat#D42460
fructose 1,6-biphosphate	Crgent Biotech	Cat# XP03590
fructose 6-phosphate	Solarbio	Cat# IF0820
guanosine 5-monophosphate	Mei5bio	Cat# G74210
O-phospho-serine	Solarbio	Cat# IP3880
Thymine	Acmecc	Cat# T13780
Critical commercial assays		
5X All-In-One RT MasterMix	AMB	Cat#G490
TC	Biosino	Cat#100020080
TG	Biosino	Cat#100020090
ALT	Biosino	Cat#000010
AST	Biosino	Cat#000020
Dual-Luciferase Reporter Assay System	Promega	Cat#E1910
CheckMate Mammalian Two-Hybrid System	Promega	Cat# E2440
Stool Genomic DNA Kit	CWBIO	Cat#CW20925
Qubit DNA Assay Kit	ThermoFisher	Cat#Q33231
Ultra DNA Library Prep Kit for Illumina	NEB, USA	Cat#E7370S
HiSeq 4000 PE Cluster Kit	Illumina	Cat#PE-410-1001

(Continued on next page)

Continued

REAGENT or RESOURCE	SOURCE	IDENTIFIER
Deposited data		
Metagenome sequencing data	This paper	BioProject ID: PRJNA1110752; BioProject ID: PRJNA1110745; BioProject ID: PRJNA1105210; BioProject ID: PRJNA1105007
RNA-seq data	This paper	GEO: GSE265852
Experimental models: Cell lines		
HEK293T	ATCC	N/A
Experimental models: Organisms/strains		
<i>Hif2a^{fl/fl}</i> and <i>Hif2a^{ΔIE}</i> mice	This paper	N/A
C57BL/6J	The Jackson Laboratory	N/A
Recombinant DNA		
Oxygen Stable pCDNA3-HIF-2 α	N/A	N/A
pBIND-HIF-2a	from Professor Yatrik M. Shah	N/A
pACT-ARNT	from Professor Yatrik M. Shah	N/A
pGL3-DMT1 Luc (HRE-Luc)	N/A	N/A
pCMV-Tag4-HIF-2aG324E+S305M	N/A	N/A
Software and algorithms		
GraphPad Prism version 9.0	GraphPad Software	https://www.graphpad.com/updates/prism-900-release-notes
ImageJ	N/A	https://imagej.net/
IBM SPSS Statistics 26.0	IBMCorp	https://www.ibm.com/support/pages/downloading-ibm-spss-statistics-26
Other		
Rodent Diet With 60 kcal% Fat	Research Diets Inc	Cat# D12492
Quaternary HPLC System	Agilent	Cat#1200 Infinity
HyperSep C18 SPE Column	Thermo	Cat#60108

RESOURCE AVAILABILITY**Lead contact**

Further information and requests for resources and reagents should be directed to the lead contact, Yanli Pang (yanlipang@bjmu.edu.cn).

Materials availability

This study did not generate new unique reagents. Materials in this work are available from the [lead contact](#).

Data and code availability

- Data availability: Metagenome data for is available through NCBI (<https://ncbi.nlm.nih.gov>) at BioProject ID: PRJNA1110752 (mice with MAFLD before and after TRF), BioProject ID: PRJNA1105007 (patients with MAFLD before and after TRF), BioProject ID: PRJNA1105210 (patients with MAFLD before and after 5A2F), and BioProject ID: PRJNA1110745 (16S RNA for mice with ATM or ATM without *R. torques*). RNA-seq data have been deposited at GEO: GSE265852.
- This paper does not report original code.
- Unprocessed data in this manuscript are available as Source Data. [Tables S1](#), [S2](#), and [S3](#) and figures are available as [supplemental information](#).
- Any additional information required to reanalyze the data reported in this paper is available from the [lead contact](#) upon request.

EXPERIMENTAL MODEL AND SUBJECT DETAILS**Human subjects and sample collection**

The human studies were all approved by the Ethics Committee of Beijing Chao-Yang Hospital, Capital Medical University ([ClinicalTrials.gov](https://clinicaltrials.gov) ID: NCT04795973). We recruited individuals with MAFLD (HSI \geq 36) from Beijing Chao-Yang Hospital, Capital

Medical University for an intermittent fasting intervention between April 2021 and April 2022. The exclusion criteria were: diet therapy before participation, pregnancy, severe hepatic diseases (cirrhosis, hepatocellular carcinoma and acute liver injury); severe nephropathy; organic digestive diseases; autoimmune diseases; cancer; infectious diseases, including pulmonary tuberculosis and AIDS; alcoholism; continuous antibiotic use for over 3 days within 3 months prior to enrollment; continuous use of a weight-loss drug for over 1 month; gastrointestinal surgery. Human serum and feces samples were collected at baseline and after the 1-month intervention. Venous blood samples were collected after overnight fasting. And the blood samples were placed at room temperature for 30 minutes, then centrifuged at $3000 \times g$ for 20 minutes. Feces samples were collected and immediately frozen in dry ice and stored at -80°C . In the time-restricted eating (TRE) intervention, all subjects participated in the 10-h TRE for 4 weeks and were instructed to eat *ad libitum* from 7 am to 5 pm and fast from 5 pm to 7 am the next day. During the 10-h eating windows, there were no restriction on types and quantities of food, and during the fasting period, participations were encouraged to drink sufficient water. As for the 5:2 intermittent fasting (5A2F) regimen, the subjects accepted the intermittent fasting intervention for 4 weeks and chose two non-consecutive days per week to eat very little and eat *ad libitum* the other 5 days of the week. The morphological indexes (height, weight, waist circumference, hip circumference, body fat percentage, the waist to hip ratio and body mass index), blood pressure, heart rate, and blood biochemical index and other indicators before and after the intervention were analyzed and recorded. The specific information of participants is shown in the [Tables S1](#) and [S2](#).

Mice and treatments

Male C57BL/6J wild type mice were purchased from Gem Pharmatech, Nanjing. All mice were randomly assigned to experimental groups and mice within experiments were age matched without presenting differences in body weights before the treatments. All mice were housed in SPF facility at a controlled temperature ($23 \pm 2^{\circ}\text{C}$) and kept in a 12-h light-dark cycle. All animal experiments were approved by the Animal Research Ethics Committees of Peking University.

8-week-old mice were fed with high-fat diet (60% kcal from fat, D12492, Research Diets) for 8 weeks to induce hepatic steatosis. For the MASH model, 8-week-old male C57BL/6J wild type mice were fed with CDAA-HFD (A06071302, Research Diets) for 8 weeks.

To explore the effect of gut microbiome in the TRF, mice were treated with antibiotics cocktail (Abx: 0.5mg/ml vancomycin, 1mg/ml metronidazole, 1mg/ml kanamycin, 1mg/ml ampicillin) or sterile PBS in water. For TRF intervention, mice were fed with a HFD for 10 hours from ZT13 to ZT23 where ZT0 was light on.

To transplant *R. torques* or *C. hathewayi*, mice were pretreated with antibiotics for 3 days and fed with a HFD, PBS, *R. torques* (10^8 CFU/mouse) or *C. hathewayi* (10^8 CFU/mouse) were gavaged every 3 days for 8 weeks. To explore the effect of *R. torques* on the pathway of intestinal epithelial cell, 8-week-old mice were treated with a HFD and PBS or *R. torques* for 2 weeks.

To establish defined microbiomes, the equivalent of different bacterium was mixed and gavaged to mice, which contained $10^7 \sim 10^8$ CFU/mouse.

To research the effect of intestinal HIF-2 α in the *R. torques*-mediated improvement of hepatic steatosis, mice received a small intestinal lentiviral injection to overexpress HIF-2 α in the ileum as previously described to induce MASLD.⁴⁶ Briefly, the ileum was elevated from 6–8 cm distal to the cecum and was ligated with vascular clamps at both ends to block distribution of lentivirus and intestinal fluids. The intestinal portion was cut with a longitudinal 3 mm incision, then flushed with saline by an insulin needle inserting right below the 6 cm ligation, and 0.2 mL lentivirus expressing HBLV-Zs Green PURO or HBLV-m-Epas1-3xflag-Zs Green PURO (both at 1.0×10^8 TU/mL; 20 μL lentivirus was diluted with saline into a total volume of 200 μL for injection) was administered via an insulin needle. 20 minutes later, vascular clamps were removed and the intestine was flushed with 200 μL saline. After that, the incision was sutured with 10-0 suture. One week later, the mice were fed with a HFD and PBS or *R. torques* (10^8 CFU/mouse) by gavage every 3 days for 8 weeks. 8-week-old male littermate *Hif2a^{fl/fl}* and *Hif2a^{ΔIE}* mice fed with a HFD and PBS or *R. torques* (10^8 CFU/mouse) by gavage every 3 days for 8 weeks.

To study the effect of HMP on the progression of hepatic steatosis, 8-week-old male C57BL/6J wild type mice were fed a HFD and treated with HMP (100 mg/L) or PBS by gavage three times per week for 8 weeks. 8-week-old male littermate *Hif2a^{fl/fl}* and *Hif2a^{ΔIE}* mice fed with HFD and HMP (100 mg kg^{-1}) or PBS by gavage three times per week for 2 weeks to explore the effect of HMP on ceramide synthesis. For transplanting *E. coli* BL21-*rtMor*, 8-week-old male C57BL/6J wild type mice were fed with HFD and *E. coli* BL21 (10^8 CFU/mouse) or *E. coli* BL21-*rtMor* (10^8 CFU/mouse) for 8 weeks.

To explore the effect of *R. torques* or HMP on the progression of MASH, 8-week-old male C57BL/6J wild type mice were fed with CDAA-HFD for 8 weeks. At the same time, PBS, *R. torques* (10^8 CFU/mouse) or HMP (100 mg/L) were administered. As for the therapy model, mice were fed with 5 weeks, and then, PBS, *R. torques* (10^8 CFU/mouse) or HMP (100 mg/L) were treated for another 3 weeks.

For the ceramide supplement experiment, mice were pretreated with antibiotics for 3 days and fed with a CDAA-HFD. PBS or *R. torques* (10^8 CFU/mouse) were gavaged every 3 days for 8 weeks. Meanwhile, ceramide (d18:1/16:0) was intraperitoneal injected every other day at the dose of 10 mg/kg.

Microbe strains and culture

The *R. torques* was purchased from BNCC (bncc360706) and cultured in brain heart infusion (BHI) broth medium in 37°C anaerobic incubators. For *in vivo* experiments, the bacteria were centrifuged at 10,000 rpm at 4°C for 3 minutes when the OD_{600} reached 0.6 and resuspended in sterile PBS to gavage mice. The bacteria were stored at 4°C for use.

E. coli BL21 was purchased from Beijing Zoman Biotechnology Co., Ltd to overexpress the 4-methyl-2-oxopentanoate reductase gene of *R. torques* (*rtMor*). *E. coli* BL21 and *E. coli* BL21-*rtMor* was streaked onto Lysogeny broth (LB) agar plates in 37°C for overnight. A single colony was put into 5 mL LB medium and cultured overnight.

Each bacterium was cultured in Gifu Anaerobic Medium (GAM) media for 48 hours at 37°C anaerobic incubators, and then diluted in fresh GAM media. Different bacterium was normalized for density by OD₆₀₀. For inoculation into mice, the equivalent of different bacterium was mixed and gavaged to mice, which containing 10⁷~10⁸ CFU/mouse.

METHOD DETAILS

DNA extraction

Genomic DNA from human feces samples or *R. torques* were isolated by using cetyltrimethylammonium bromide (CTAB, a cationic detergent). In brief, 50 mg of the feces samples or bacteria were weighed and homogenized in 600 μL TE buffer and centrifuged at 10,000×g for 10 minutes. The precipitation was incubated with 2×CTAB at 60°C for 30 minutes, and then extracted by chloroform:isopentanol (24:1). The isolated genomic DNA was prepared for metagenomics sequencing and bacteria-specific real-time quantitative PCR.

Metagenomics sequencing

Metagenomics sequencing was described previously.⁴⁷ 700 ng DNA per samples was used for DNA sample preparation. Sequencing libraries were generated by NEB Next Ultra DNA Library Prep Kit for Illumina; the manufacturer's recommendations and index codes were adopted to annotate sequences in each sample. The fragmented DNA was end-repaired, polyA-tailed and ligated with a sequencing adaptor for Illumina sequencing. PCR amplification and DNA purification were performed with an AMPure XP system. The DNA concentration was measured with the Qubit DNA Assay Kit in a Qubit 2.0 fluorometer and diluted to 2 ng/μL. And the library quality was assessed by using the Agilent Bioanalyzer 2100 system. Clustering of index-coded samples was performed on a cBot Cluster Generation System using a HiSeq 4000 PE Cluster Kit according to the manufacturer's instructions. After cluster generation, the libraries were sequenced on the Illumina HiSeq 4000 platform, and 150-bp paired-end reads were generated. Taxonomic composition of human metagenomes and mouse metagenomes were profiled by MetaPhlan2 and Kraken2 tools respectively.

Biochemical assays

Approximately 20 mg liver tissue was weighed, homogenized in 20× triglyceride lysis buffer and heated at 70°C for 10 minutes. Centrifuged at 2,000 rpm and the supernatant was collected. To detect the level of cholesterol and triglyceride, plasma or supernatant obtained from above step was measured by Cholesterol Assay Kit (COD-PAP Method, Biosino) and Triglyceride Assay Kit (GPO-PAP Method, Biosino). The hepatic cholesterol and triglyceride were normalized to the weight and presented as milligrams of lipid per gram of tissue weight. Plasma ALT and AST levels were measured by Alanine Transaminase Kit (Alanine Substrate Method, Biosino) and Aspartate Aminotransferase Kit (Aspartate Substrate Method, Biosino), respectively.

Histological analysis

Liver tissues were fixed in 4% paraformaldehyde for 4-6 hours and embedded with paraffin, stained by H&E or Sirius red. And optimal cutting temperature compound (OCT)-embedded frozen liver sections were stained by Oil Red O.

Real-time quantitative PCR analysis and RNA-seq profiling

Total RNA of mouse intestine tissue was isolated with Trizol reagent (15596018, ambion). cDNA was synthesized from 2 μg of total RNA with 5×All-In-One RT MasterMix (G592, abm). Real-time PCR primer sequences are listed in Table S3. The relative amount of each mRNA was calculated by normalizing to the corresponding 18S mRNA. The results were presented as fold change relative to control group. The relative amount of bacteria DNA was calculated by normalizing to the corresponding 16S rDNA.

Library preparation and transcriptome sequencing was conducted by Novogene LLC. NEBNext Ultra™ RNA Library Prep Kit for Illumina (NEB, USA) was used to prepare the sequencing libraries. The libraries were sequenced on Illumina HiSeq platform to generate 150bp paired-end reads. Adapter trimming and low-quality reads removing was conducted by Trim Galore v0.6.7. Clean reads were aligned to the mouse genome mm10 with Hisat2 v2.2.1. Counts of each gene were quantified using featureCounts v2.0.1. Differential expression analysis was performed by edgeR v3.38.4 R package. Thresholds for differential expression were set as follows: adjusted p-value of 0.05, absolute value of fold change of 1.5. Gene Ontology enrichment analysis and transcription factor enrichment analysis was performed by clusterProfiler v4.4.4 R package.

Metabolomics analysis

For plasma samples, 20 μL plasma was mixed with 30 μL sterile water and 200 μL cold chloroform:methanol (2:1) containing 1.25 μM Ceramide (d18:1/19:0) as the internal standard. The mixture was vortexed for 20 seconds and placed on the ice for 30 minutes. After centrifugation at 13,000 rpm for 20 minutes at 4 °C, the lower organic phase was collected and concentrated by termovap sample concentrator. The samples were dissolved in 100 μL acetonitrile:isopropanol (1:1) and vortexed for 60 seconds. For extracting ceramides of intestinal epithelial organoid medium, 50 μL medium was mixed with 200 μL cold chloroform:methanol (2:1) containing 1.25 μM Ceramide (d18:1/19:0) as the internal standard. For lipidomics analysis of intestine epithelial tissue and organoid,

approximately 20 mg tissue or total organoid was homogenized in 100 μ L sterile water, and then centrifuged at 10,000 rpm for 10 minutes. The protein concentration of supernatant was measured and 100 μ L supernatant was mixed with 900 μ L cold chloroform:methanol (2:1) containing 1.25 μ M Ceramide (d18:1/19:0) as the internal standard. The followed steps were mentioned above. The concentration of tissue ceramides was normalized to the protein weight. Samples were analyzed by Eksigent LC100 coupled with Triple TOF 5600 system (AB SCIEX, Concord, ON, Canada) using a Waters XBridge Peptide BEH C18 column (3.5 μ m, 2.1 \times 100 mm; Waters Corporation, USA). The mobile phase was a mixture of 99.9% water (A) and 49.95% acetonitrile and 49.95% isopropanol (B) both containing 10 mM ammonium formate and 0.1% formic acid. The flow rate was 0.4 mL/min, and the gradient elution was performed as followed: 35% B at 0 min, 80% B at 2 min, 100% B at 9 min, 100% B at 15 min, and 35% B at 16 min, and 35% B at 20 min. The injection volume was 2 μ L. All the lipid molecules were identified through the acknowledged database Lipidmaps (<http://www.lipidmaps.org>) and the comparison with the standards (including retention time, parent ion mass and MS/MS fragmentations). Peak extraction and integration were performed with PeakView1.2 software. For quantitation of sphingolipid metabolites, the data was analyzed by MultiQuant 2.1 software (AB SCIEX).

Luciferase reporter gene assays

The HEK293T cells were seeded into a 24-well plate at a cell density of 1×10^4 cells per well. The cells were co-transfected with HIF-2 α plasmid, p2.1 luciferase reporter plasmid and Renilla luciferase (pRL-luciferase) plasmid by Lipofectamine 3000 transfection reagent. After 24-hour transfection, the cells were exposed to PT2385 and different concentrations of HMP for 24 hours and then the cells were lysed by reporter lysis buffer. Luciferase assays were performed using the Dual-luciferase assay system. For screening the effect of metabolites of *R. torques* on HIF-2 α /Arnt heterodimer transcription, the medium was filtered by a 1 KDa centrifugal filter to obtain the >1 KDa protein segment and small molecules segment. To identify the mechanism of HMP influencing HIF-2 α /ARNT heterodimer transcription, two PT2385 binding sites in the mouse HIF-2 α were mutated to generate mHIF-2 α G323E+S304M.¹⁶ To investigate the role of HMP on HIF-2 α /ARNT interaction, mammalian two-hybrid system was performed as previously described. The HEK293T cells were co-transfected with pG5 luciferase vector, pBIND-HIF2 α and pACT-ARNT vector (gifted from Professor Yatrik M. Shah). After transfected for 24 hours, the cells were exposed to HMP for 36–48 hours, and the assays were performed as the protocol described in CheckMate™ Mammalian Two-Hybrid System.

Co-immunoprecipitation and western blotting

The HEK293T cells were cultivated in 10-cm culture dish. The cells were co-transfected with HIF-2 α and ARNT plasmids. After 24-hour transfection, the cells were exposed to HMP for 24 hours. Cells were incubated in NP40 buffer addition with protease inhibitor cocktail for 30 minutes on ice, and then the cells were collected and cracked by ultrasonic machine. The fragments were centrifuged at 13,000 rpm for 15 minutes at 4°C. The supernatants were separated to two parts. One part was mixed with 5 \times protein loading buffer and boiled for 5 minutes as the input. The other part was immunoblotted overnight at 4°C with agarose beads and HIF-2 α antibody. Then the beads were washed by TBST for three times and dissolved by protein loading buffer. The intestinal tissues were homogenized in RIPA buffer with protease and phosphatase inhibitors. The protein extracts were separated by sodium dodecyl sulfate (SDS)-polyacrylamide gel (PAGE) electrophoresis on a 10% running gel and transferred to a polyvinylidene fluoride (PVDF) membrane. The membrane was blocked with 5% defatted milk and incubated with antibodies against HIF-2 α (NB100-122, Novus), ARNT (sc-55526, Santa Cruz) overnight at 4°C.

HMP level measurements

Concentrations of HMP were measured by LC-MS/MS. About 20 mg fecal samples were homogenized after addition of 200 μ L 80% methanol (including 5% formic acid). Following mixing rapidly, the mixture was left on ice for 15 minutes. The supernatant was filtered by 0.22 μ m syringe filter after centrifuging for 10 minutes at 13000 \times g. 5 μ L was analyzed by QTRAP 5500 system (AB SCIEX, Concord, ON, Canada) using an Acquity UPLC CSH column (2.1 \times 100 mm, 1.7 μ m; Waters Corporation, USA). The mobile phase was water containing 0.1% formic acid (A) and acetonitrile containing 0.1% formic acid (B), with a constant flow rate (0.25 mL/min). The analytes were separated by gradient elution: 0 \rightarrow 0.5 min, 20% B; 0.5 \rightarrow 3 min, 20 \rightarrow 60% B; 3 \rightarrow 4 min, 60% B; 4 \rightarrow 6 min, 20% B. The analytes were measured at m/z 131.1 \rightarrow 85.1 under negative mode.

QUANTIFICATION AND STATISTICAL ANALYSIS

GraphPad Prism version 8.0 (GraphPad Software, San Diego, CA) was used for statistical analysis. The experimental data were shown as the mean \pm SEM values. The investigators involved in the study were not completely blinded in each experiment during sample collection and analysis. The sample size was estimated on the basis of previous experience, sample availability and previously reported studies.⁴⁸ No data were excluded from the data analysis. The normal distribution of the data was determined by the Shapiro-Wilk normality test. For statistical comparisons, Student's t test or one-way ANOVA with Tukey's test was used to compare normally distributed variables. Wilcoxon's Sign Rank Test was used to compare paired samples. Non-normally distributed data were

compared by the Mann-Whitney U test (between two groups) or the Kruskal-Wallis test (among multiple groups). Wilcoxon matched-pairs signed rank test was used for clinical participants. For metagenomics data, the adj. p value threshold was calculated using the moderated Student's t test followed by the Benjamini-Hochberg procedure for multiple testing correction via the false discovery rate (FDR). Spearman's rank tests between changes in microbial species and host metabolome were calculated based on species with significant differences between the two groups. Benjamini-Hochberg procedure with a cutoff of 0.1 was applied to all Spearman's rank tests. $p < 0.05$ was considered significant. Correlation analysis of the gut microbiome and host metabolome was performed by the Spearman's rank tests.